Interactions between lattice dislocations and twin boundaries in tungsten: A comparative atomistic simulation study

Matous Mrovec, Christian Elsaesser, Peter Gumbsch

Interactions between lattice dislocations and twin boundaries in tungsten: A comparative atomistic simulation study

Journal:	*Philosophical Magazine & Philosophical Magazine Letters*
Manuscript ID:	TPHM-09-Jun-0272.R1
Journal Selection:	Philosophical Magazine
Date Submitted by the Author:	04-Aug-2009
Complete List of Authors:	Mrovec, Matous; University of Karlsruhe, IZBS; Fraunhofer Institute for Mechanics of Materials Elsaesser, Christian; University of Karlsruhe, IZBS; Fraunhofer Institute for Mechanics of Materials Gumbsch, Peter; University of Karlsruhe, IZBS; Fraunhofer Institute for Mechanics of Materials
Keywords:	atomistic simulation, dislocations, grain boundaries, tungsten
Keywords (user supplied):	atomistic simulation, dislocations, grain boundaries

Philosophical Magazine
Vol. 00, No. 00, 21 March 2009, 1–14

RESEARCH ARTICLE

Interactions between lattice dislocations and twin boundaries in tungsten: A comparative atomistic simulation study

M. Mrovec[a,b*] , C. Elsässer[a,b] and P. Gumbsch[a,b]

[a]IZBS, University of Karlsruhe, Kaiserstr. 12, 76131 Karlsruhe, Germany
[b]Fraunhofer Institute for Mechanics of Materials IWM, Wöhlerstr. 11, 79108 Freiburg, Germany

(*June 23, 2009*)

Plastic deformation of polycrystalline materials is largely controlled by the interaction between lattice dislocations and grain boundaries. The atomistic details of these interactions are however difficult to discern even by advanced high-resolution electron microscopy methods. In this paper we study several interactions of screw and edge dislocations with two symmetric tilt grain boundaries in the body-centred cubic metal tungsten by atomistic simulations. Two distinct models of interatomic interactions are applied - an empirical Finnis-Sinclair (FS) potential and a bond-order potential (BOP), which is based on quantum mechanical principles within the tight-binding electronic-structure theory. Our study shows that the outcome of the interactions is sensitive to the employed interatomic potential. Origins of the deviating behavior can be traced to differences in the description of atomic bonding by the two potentials. Independent of the employed interatomic potential, the simulations reveal that simple empirical criteria for dislocation transmission, which are based on geometry and stress arguments only, do not apply in general. Instead, in most cases processes occuring at the atomic level play a decisive role in determination of the underlying mechanisms of dislocations/grain-boundary interactions.

1. Introduction

When a polycrystalline metal undergoes plastic deformation, a large number of lattice dislocations impinge on grain boundaries (GBs) and interact with them. It has been observed experimentally that the interactions can result in impediment, transmission, absorption and reemission, or even reflection of dislocations [1, 2]. Unfortunately, little information is available about details of these processes at the atomic scale and only simple empirical criteria based on elementary geometry and stress factors have been proposed to predict the outcome of the dislocation/grain-boundary (DGB) interactions [3, 4]. While these criteria apply in some cases, a number of experimental [5–11] and theoretical [12–27] studies have shown that they are not valid in general and that the mechanisms of the DGB interactions are influenced by processes occuring at the atomic level.

In this work we investigate several DGB interactions in the bcc transition metal tungsten by atomistic simulations. Tungsten was chosen as our model material because of its peculiar mechanical behavior, which is controlled to a great extent by the structure and properties of extended defects, namely dislocation cores and grain boundaries. Depending on external conditions such as temperature, strain rate, or load orientation this transition metal can deform plastically by slip or deformation twinning or it can fracture by predominantly intergranular cleavage [28]. Properties

*Corresponding author. Email: matous.mrovec@iwm.fraunhofer.de

ISSN: 1478-6435 print/ISSN 1478-6443 online

DOI: 10.1080/1478643YYxxxxxxxx
http://www.informaworld.com

of dislocations, GBs, and details of mutual interactions between these extended defects are therefore of great interest since they may provide valuable information about conditions under which the competing deformation mechanisms take place.

The most important precursor of all atomistic simulations is a reliable description of interatomic interactions. Calculations of complex phenomena such as the DGB interactions require large simulation blocks and careful handling of boundary conditions. These stringent computational demands necessitate employment of empirical interatomic potentials instead of accurate first-principles electronic structure methods. To our knowledge almost all previous DGB simulations were performed with simple empirical potentials of the embedded-atom-method or Finnis-Sinclair (FS) type [12–17, 20–27, 29–32] with the exception of a recent work of Katzarov et al. on TiAl [33].

In the present paper we perform the simulations with two distinct models of interatomic interactions – an empirical Finnis-Sinclair potential [34, 35] and a recently developed bond-order potential (BOP) [36]. The FS potential is a many-body central-force scheme which has been used extensively in atomistic studies of extended defects in metals because of its simplicity and computational efficiency. Nevertheless, it is unable to describe properly the directional covalent bonds that are primarily responsible for structural and cohesive properties of bcc transition metals [36–41]. In order to validate FS results we therefore repeated the simulations with the BOP model, which is based on the real-space parameterized tight-binding (TB) method and provides implicitly a correct description of the angular character of bonding originating from d-electrons. An important advantage of the BOP scheme for simulations of extended defects and their interactions is that unlike classical TB models it scales linearly with the size of system since the diagonalization of the Hamiltonian matrix is replaced by direct calculation of the bond order in real space [42–44].

The main goals of the present work are twofold. First, we investigate the atomic-level mechanisms associated with the DGB interaction processes and compare the simulation results with predictions of the empirical criteria for dislocation transmission. Second, we examine if the outcome of the interactions depends on the interatomic potential employed and analyze underlying causes of eventual differences.

2. Simulation methodology

The DGB interactions were investigated for two symmetric tilt grain boundaries with a common $[\bar{1}10]$ tilt axis, namely, $\Sigma3(11\bar{2})$ and $\Sigma3(111)$. These GBs were chosen as model systems since extensive plastic deformation of bcc metals (e.g. during wire drawing) leads to a strong preferential $\langle 110 \rangle$ texture [45, 46]. Both GBs are high-angle GBs with a high density of coincidence sites and well defined equilibrium atomic structures. Their energies are however largely different (see below) and they can be therefore considered as representative cases of low and high energy GBs.

Configurations investigated in this work present rather special cases among possible DGB interactions in which the cross slip should encounter only a small resistance. In all our simulations the dislocation line lies parallel to the GB plane while the glide plane, i.e. the maximum resolved shear stress (MRSS) plane on which the dislocation is forced to glide, is always perpendicular to the GB plane. Because of the mirror-symmetrical structure of both GBs the glide plane continues through the GB into the other grain and the slip systems in both grains are therefore completely equivalent. Based on geometry considerations, the GBs in this case should

Table 1. Main characterictics of the four DGB configurations investigated in this work (see also figure 1).

Case	GB	Dislocation type	Slip systems in the grains
A	$\Sigma3(11\bar{2})$	screw	$[111](\bar{1}10)$ / $[11\bar{1}](\bar{1}10)$
B	$\Sigma3(111)$	edge	$[111](\bar{1}10)$ / $[11\bar{1}](\bar{1}10)$
C	$\Sigma3(111)$	edge	$[\bar{1}\bar{1}\bar{1}](\bar{1}\bar{1}2)_{\mathrm{ATW}}$ / $[\bar{1}\bar{1}1](112)_{\mathrm{TW}}$
D	$\Sigma3(111)$	edge	$[111](\bar{1}\bar{1}2)_{\mathrm{TW}}$ / $[11\bar{1}](112)_{\mathrm{ATW}}$

not act as obstacles to slip propagation because no residual GB dislocations are necessary to compensate for a change of the slip system.

For the chosen GBs there exist four such cases of DGB interactions, in which the $1/2\langle111\rangle$ dislocation of either pure screw or pure edge type impinges in parallel orientation on the GB. The four possibilities are described in table 1. In case A, a $1/2[111]$ screw dislocation gliding on a $(\bar{1}10)$ plane interacts with the $\Sigma3(11\bar{2})$ GB. In the remaining three cases an edge dislocation with the same Burgers vector gliding on either $(\bar{1}10)$ or $(\bar{1}\bar{1}2)$ planes interacts with the $\Sigma3(111)$ GB. For the $\{112\}$ glide planes it is necessary to distinguish between the twinning (TW) and antitwinning (ATW) directions. Since the $(\bar{1}\bar{1}2)$ plane is not a mirror plane the shearing of the crystal as well as the dislocation glide in opposite $1/2[111]$ directions are not equivalent. Furthermore, even though the $(\bar{1}\bar{1}2)$ plane continues through the GB the sense of shear is reversed, i.e. the TW sense in the left bicrystal changes to the ATW sense in the right bicrystal and vice versa. These two possibilities need to be treated separately and correspond to cases C and D.

The computational procedure was the same in all simulations. Initially, the GBs were created in the centre of the simulation cell and they were fully relaxed to their equilibrium configurations. After the static relaxation of the GB atomic structure either a perfect screw or edge dislocation with the $1/2\langle111\rangle$ Burgers vector was introduced in the middle of one of the grains. At this distance no attractive or repulsive forces were detected between the dislocation and the GB in any of the investigated systems.

With the dislocations present, the blocks were again fully relaxed. During the relaxation the positions of the dislocation cores remained at their initial elastic centers. It should be noted that tungsten is almost elastically isotropic and that incompatibily stresses at GBs are therefore negligible. Consequently, there are no long-range elastic forces on the dislocations near the GBs.

In the final step, a homogeneous shear strain was imposed on the simulation block, corresponding to a shear stress as prescribed by anisotropic elasticity theory. The shear stress was applied in the direction of the Burgers vector in such a way that the dislocation was forced to move towards the GB. The shear strain was gradually increased in small increments and the block was fully relaxed after each step so that the simulations were done effectively at 0 K.

The simulation setup with the sense of shear for both dislocation types is shown schematically in figure 1. The size of the simulation box was typically 15 nm $\times$ 10 nm in the x and y directions and the number of atoms ranged between 5 and 10 thousand. We carried out additional simulations with larger blocks using only the FS potential but did not find any size effect. Periodic boundary conditions were imposed along the z direction parallel to the dislocation line while fixed boundary conditions were used in the perpendicular x and y directions. The block in the x and y directions then consisted of an active region, in which all the atoms are fully relaxed, and an fixed region where the atoms are permanently displaced in accordance with the anisotropic elastic field of the dislocation. In order to allow the GB dislocations to move freely along the GB, simulations with free top and bottom surfaces were also tested. Again, the results were qualitatively the same as

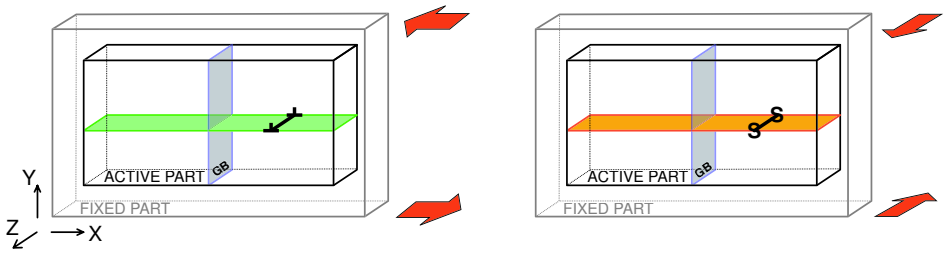

Figure 1. A schematic diagram of the simulation setup for the DGB interactions with edge and screw dislocations; the sense of applied shear is marked by arrows.

those with fixed boundaries.

3. Results

3.1. *Properties of the grain boundaries*

Since the atomic structure and energetics of the GBs may influence the outcome of the DGB interactions we computed first several characteristic properties of the two GBs using both FS and BOP schemes and compared them to results of benchmark first-principles density-functional theory (DFT) calculations [36, 47]. Here, we focus mainly on the $\Sigma3(11\bar{2})$ GB since, as will be discussed later, the differences in the description of this boundary by the two interatomic potentials are likely to be linked to differences in the observed DGB interactions.

The $\Sigma3(11\bar{2})$ GB is associated with deformation twins in bcc metals and is therefore frequently present in materials deformed at low temperatures or high strain rates [6]. Due to its regular atomic structure and bulk-like atomic density it is the lowest energy boundary among the [110] symmetric tilt GBs in bcc transition metals. The structure and energetics of this GB have been investigated extensively in the past for various bcc metals, both theoretically and experimentally (see, e.g., Refs. [37, 47–51] and references therein). A general result of all previous studies is that there exist two possible equilibrium configurations of this boundary, whose energies are nearly degenerate. The first configuration is a mirror symmetric structure corresponding to the coincidence site lattice interface [2]. The second configuration is obtained from the first one by displacing the upper grain with respect to the lower grain parallel to the boundary plane by the vector $\mathbf{t} = 1/12[111]$. The two structures are known as "reflection" and "isosceles" GBs [49], respectively, and are shown in figure 2.

The [111] lateral grain translation not only distinguishes the two low-energy GB structures but is of primary interest because it coincides with the direction of the twinning shear during deformation twinning. The computed energy profiles associated with the lateral translation of the two grains in the [111] direction over the whole GB period are plotted in figure 2. The curves in the figure represent the variation of the energy for rigid relative displacements of the grains without any atomic relaxation. The full symbols mark the energies of three high-symmetry translation states with all atomic positions relaxed. Figure 2 shows that except of the two low-energy configurations there exists another symmetry-dictated metastable configuration of this boundary, which can be obtained from the isosceles structure by a translation $\mathbf{t} = 1/4[111]$. This transition structure corresponds to an energy maximum and is therefore a hypothetical configuration which is unlikely to be present in the real material. This configuration may be however encountered as a transition state during shearing of the crystal.

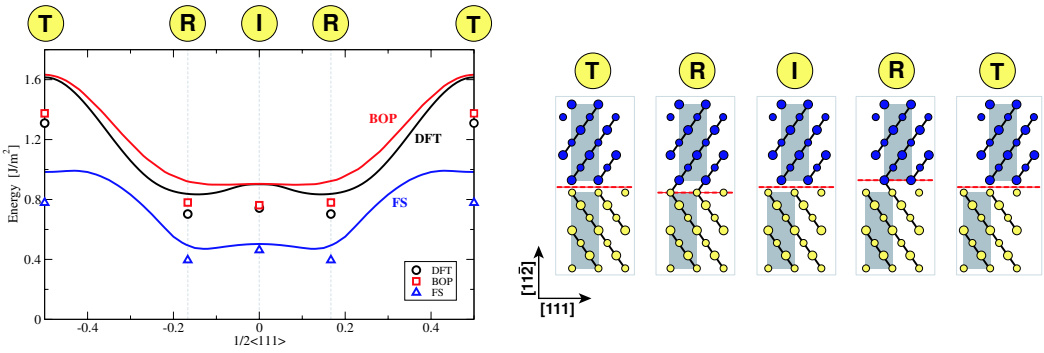

Figure 2. Energy of the $\Sigma3(11\bar{2})$ GB as a function of lateral displacement the grains along the [111] direction. The curves correspond to rigid relative displacements of the grains without any relaxation and the full symbols to fully relaxed symmetry structures. The corresponding atomic structures of the metastable GBs along the tilt axis are depicted next to the graph. Atoms with different radii lie in different $(\bar{1}10)$ planes; symbols R, I, and T denote reflection, isosceles, and transition structures, respectively.

Table 2. Comparison of GB energies for the $\Sigma3(11\bar{2})$ and $\Sigma3(111)$ boundaries calculated by different methods. For the $\Sigma3(11\bar{2})$ GB energies of the reflection (R), isosceles (I), transition (T) structures, and the difference between T and R structures are listed separately. All values are in mJ/m^2

GB	DFT	BOP	FS
$\Sigma3(11\bar{2})$			
(R)eflection	703	780	395
(I)soscelles	743	762	462
(T)ransition	1310	1375	778
Δ_{T-R}	607	595	383
$\Sigma3(111)$			
3D PBCs (12 atom cell)	2274	2195	1401
3D PBCs (24 atom cell)	2350	2409	2337
2D PBCs	–	2398	2364

Since the calculations can be carried out also with accurate first-principles methods, they serve as a valuable benchmark case for validation of the employed interatomic potentials (cf. Refs [38, 47]). The comparison in figure 2 shows that for rigid displacements the BOP results follow closely those of DFT both qualitatively and quantitatively. The FS potential mimics correctly the shape of the energy profile but the absolute values are underestimated by almost factor of two. After relaxation the DFT calculations yield the reflection structure to be the most stable. According to the BOP calculations, both the isosceles and reflection structures are metastable with the isosceles structure favored by 18 mJ/m^2 over the reflection structure (see table 2). Hence, in the prediction of the ground state structure DFT and BOP give contradictory results, although the energy difference is very small and represents only about 2 % of the GB energy. The FS potential gives correctly the order of the three GB structures but significantly underestimates their absolute energies. Additionally, the energy barrier related to the shear strength of the GB along the [111] direction, i.e., the energy difference between the transition and reflection structures, is also predicted to be about 40% lower than in DFT and BOP calculations (see table 1). The reason for these strong underestimations is the central-force character of the FS potential. In the $\Sigma3(11\bar{2})$ boundary the separation of the first and second neighbours is the same as in the ideal crystal and thus only the third and more distant neighbours contribute to the GB energy.

In contrast to the $\Sigma3(11\bar{2})$ GB, the atomic structure of the $\Sigma3(111)$ deviates markedly from the bulk bcc environment and its energy is therefore significantly higher than that of the former boundary (see table 2). We found that all three

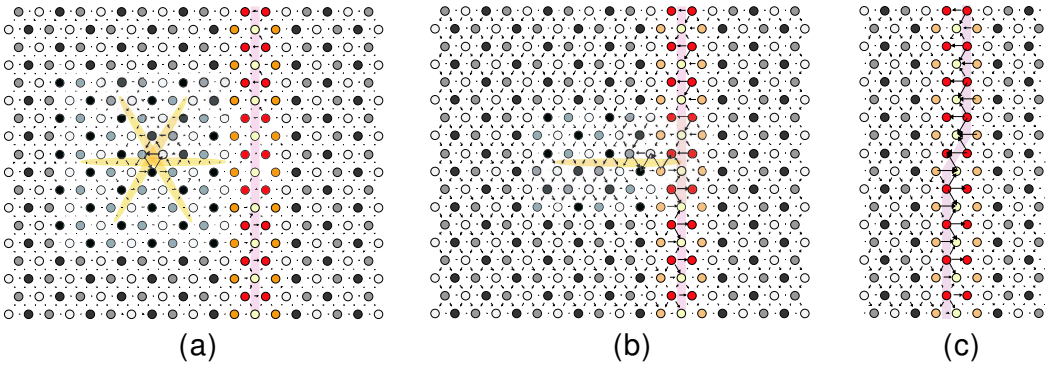

Figure 3. Initial (a), intermediate (b), and final (c) simulation snapshots from the DGB interaction between the 1/2[111] screw dislocation gliding on the $(\bar{1}10)$ plane and the $\Sigma3(11\bar{2})$ GB (BOP simulations). The pictures are $\langle 111 \rangle$ views with the $(\bar{1}10)$ glide plane lying horizontally. The arrows were obtained using the standard method of differential displacements [48] and correspond to atomic displacements in the $\langle 111 \rangle$ direction. The nonplanar structure of the dislocation core and position of the GB plane are highlited.

computational methods agree very well in predicting the GB energy as well as the atomic structure provided that the boundary is well isolated (does not interact with itself). In DFT calculations, periodic supercells containing two identical GBs are necessary and the cells must be large enough to avoid mutual interactions between the boundaries. For the $\Sigma3(111)$ GB a supercells with 12 atoms does not satisfy this requirement since the GBs are separated by only three $\{111\}$ planes and start to interact. This interaction leads to a reduction of the GB energy. The decrease is only marginal in DFT and BOP calculations, but in the case of FS potential it leads to unphysical changes in the structure of the bulk region between the GBs and a significant drop in the energy. This behavior is again likely to be caused by insufficient transferability of the FS potential to considerably distorted environments. Table 2 shows that for the 24 atom supercell, in which the distance beween periodic images of the GBs is sufficiently large, the agreement between all three methods is excellent. For BOP and FS potentials these results are also consistent with calculations done using 2D periodic boundary conditions (PBCs) parallel to the interface in which the GB is effectively embedded in two infinite bulk halfcrystals.

3.2. *Case A: Interaction between screw dislocation gliding on* $\{\bar{1}10\}$ *plane and* $\Sigma3(11\bar{2})$ *GB*

The first DGB interaction is the only one among the four investigated cases where a screw dislocation appears. It has been known for long time that properties of screw dislocations in bcc materials differ markedly from those of edge dislocations [52]. Characteristic features of the screw dislocations, such as low mobility, high intrinsic lattice friction (Peierls stress), and thermally activated motion via formation of kinks, have their origin in a three-dimensional non-planar structure of the dislocation core (for review see e.g. Refs. [40, 41, 52] and article by Vitek in this special issue).

Since the two employed interatomic potentials predict qualitatively different core structures of the 1/2[111] screw dislocation [36, 40] it may be expected that this difference will be also reflected in the DGB interaction process. Our calculations however reveal that the interaction between the 1/2[111] screw dislocation gliding on the $(\bar{1}10)$ plane and the $\Sigma3(11\bar{2})$ GB proceeds identically for both potentials. Figure 3 depicts initial, intermediate, and final configurations of the simulations using the standard method of differential displacements [48]. The screw dislocation starts moving towards the boundary [figure 3(a)] at the same critical stress as in

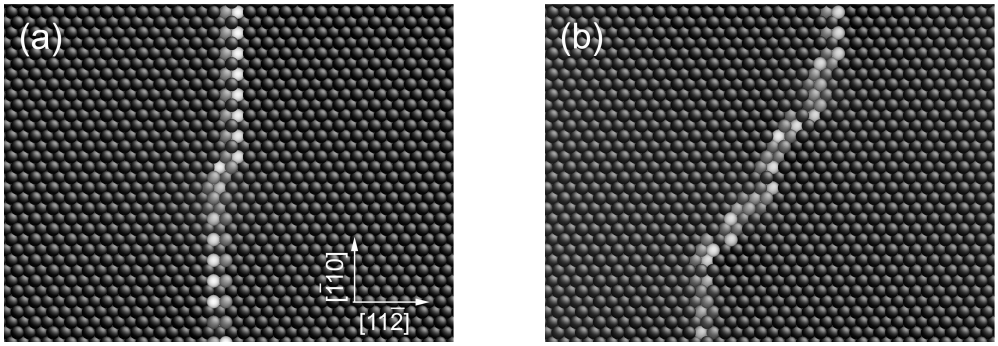

Figure 4. Structure of the $\Sigma3(11\bar{2})$ GB after interaction with one (a) and eight (b) 1/2[111] screw dislocations (FS simulation).

the bulk crystal, which confirms that the GB does not influence the Peierls barrier of the dislocation. When the dislocation reaches the GB [figure 3(b)] it is absorbed and immediately dissociates into three partial dislocations, each with the Burgers vector of 1/6[111]. These dislocations, also known as twinning dislocations which propagate deformation twins [1, 6], are geometrically admissible defects at this interface and can move conservatively along the GB plane. After the dissociation, a mutual repulsion forces two of the twinning dislocations to glide in opposite directions on neighboring $(11\bar{2})$ GB planes. As a result of this process the GB above and below the absorption site migrates in opposite directions and an embryo of a new GB, which contains the remaining twinning dislocation, forms at the interaction site [figure 3(c)].

While BOP calculations are computationally demanding, the efficiency of the FS potential enables us to study a more realistic case of DGB interaction with multiple incoming dislocations. Using free top and bottom surfaces of the simulation block so that the GB dislocations can leave the block we gradually inserted eight dislocations in the vicinity of the boundary. The simulations show that also the subsequent interactions proceed in a similiar way as with a single dislocation, i.e., by absorption and dissociation of the incoming lattice dislocations. Figures 4(a) and 4(b) depict the snapshots of the simulation block after absorption of one and eight dislocations, respectively, using the local von Mises shear strain invariant [53]. Remains of the original straight boundary plane can be seen only in the top and bottom regions of figure 4(b) with a newly formed GB in between. The new GB is inclined by about 60 degress to the original GB and is therefore itself an imperfect $\Sigma3\{112\}$ twin GB.

3.3. *Case B: Interaction between edge dislocation gliding on* $\{\bar{1}10\}$ *plane and* $\Sigma3(111)$ *GB*

Unlike the 1/2[111] screw dislocations, the edge dislocations have planar cores and, consequently, their mobility is several orders of magnitude higher than the mobility of the screws [1]. Both BOP and FS potentials give a planar core structure for the 1/2[111] edge dislocation spread on the $(\bar{1}10)$ plane and differ only in the extension of the core.

Surprisingly, despite the similar dislocation cores structures the BOP and FS potentials give qualitatively different results for the interaction between the 1/2[111] edge dislocation gliding on the $(\bar{1}10)$ plane and the $\Sigma3(111)$ GB. The initial and final snapshots of the simulation box from both simulations are shown in figure 5. In the BOP simulation the dislocation is again blocked by the GB and stays embedded in the boundary even when the shear stress is increased up to 6% of the shear elastic modulus C_{44}. The same GB in the FS simulations presents a much weaker obstacle for the dislocation. Initially, the dislocation is also absorbed at

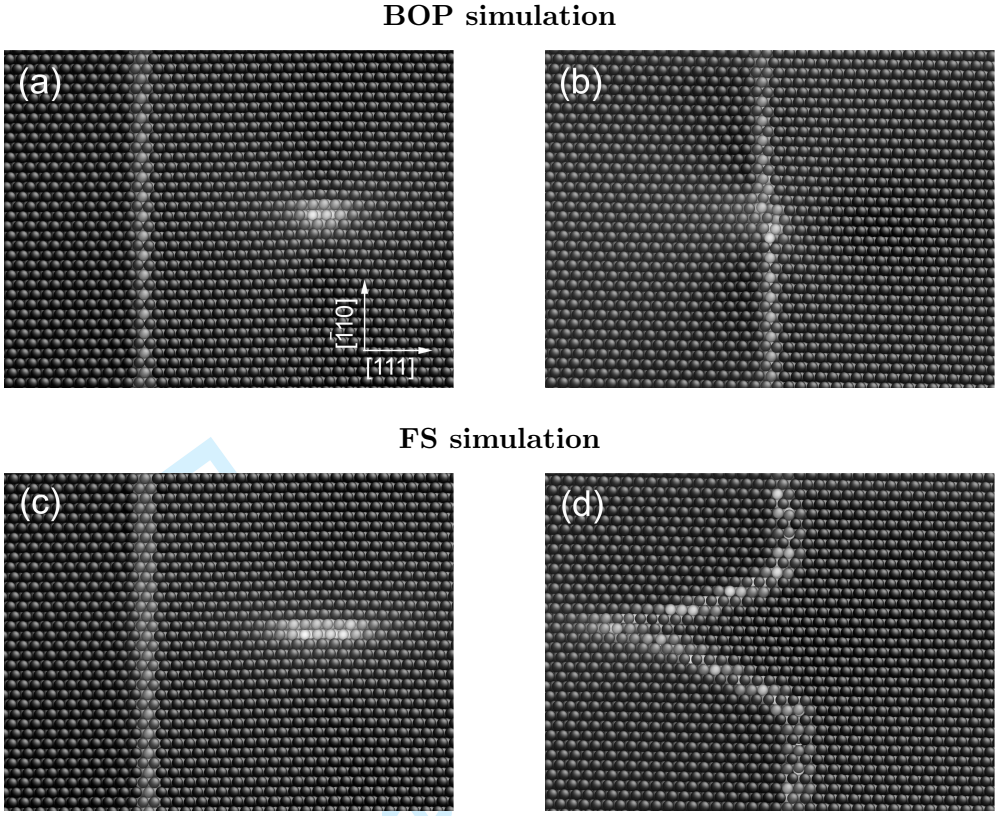

Figure 5. Initial, (a) and (c), and final, (b) and (d), simulation snapshots from the DGB interaction between the 1/2[111] edge dislocation gliding on the ($\bar{1}$10) plane and the Σ3(111) GB calculated using BOP and FS potentials, respectively.

the GB but at the applied stress of about 3% of C_{44} it detaches from the GB and starts to glide into the neighboring grain. As shown in figure 5(d), the outgoing edge dislocation triggers a wave of local changes in the crystal, which follow the moving dislocation and effectively destroy the original GB. The disintegration of the GB is caused by ongoing transformations of the ABCBAC stacking of the (111) planes across the GB to the ideal ABCABC stacking of the bulk bcc lattice. The transformation can be achieved by translating atoms on neighboring ($\bar{1}$10) planes in opposite directions by the vector ±1/6[111]. This atomic shuffling, which is schematically shown in figure 6, is associated with an energy barrier. Calculated profiles of this barrier in the ideal bcc structure are shown also in figure 6. We can see that while the magnitude of the barrier is around 4 eV according to DFT and BOP calculations, with the FS potential it reaches only 1.5 eV. The presence of the absorbed dislocation and the effect of the applied stress probably decrease the barrier even further and lead thus to initiation of the transformation.

3.4. *Cases C and D: Interaction between edge dislocation gliding on* {211} *plane and* Σ3(111) *GB*

It was shown already more than thirty years ago by Yamaguchi and Vitek [54, 55] that the core of the 1/2⟨111⟩ edge dislocation lying on a {112} plane is also planar. Since the core is predominantly confined to a single plane it can be described as a continuous distribution of the Burgers vector [26]. This distribution is asymmetric due to the well known twinning-antitwinning asymmetry of shear on {112} planes and may be interpreted as a dissociation into two fractional dislocations with the Burgers vectors 1/6⟨111⟩ and 1/3⟨111⟩ [52]. The dislocation therefore behaves differently when gliding in opposite ⟨111⟩ directions and the two cases need to be

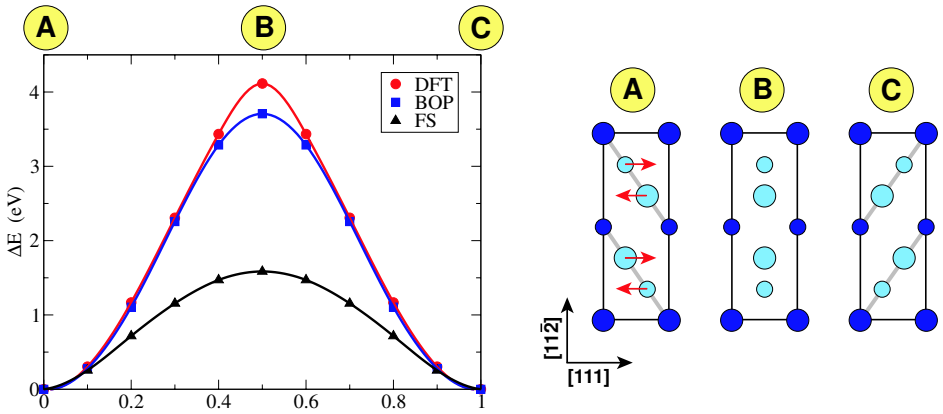

Figure 6. Calculated energy barriers associated with shuffling of atoms along the [111] direction on neighboring {$\bar{1}$10} planes. The atomic configuration corresponding to the initial, transition, and final states are shown schematically on the right.

treated separately.

Similarly as in case B, BOP and FS simulations give qualitatively different results even though the dislocation core structures from the two potentials are very similar. In BOP simulations, the result of the DGB interaction is independent of the sense of shearing. The dislocation is always trapped at the GB and does not propagate to the neighboring grain. A sequence of simulation snapshots from cases C and D are shown in figures 7 and 8, respectively.

In contrast, the outcome of the interaction in FS simulations depends on the crystal orientation. In case C, which corresponds to the ATW/TW orientation of the grains, the dislocation starts moving in the right grain in the antitwinning direction while the sense of shear in the neighboring grain is reversed to the twinning direction. Figure 7(e) shows that when the dislocation approaches the GB the compressive stress field above its glide plane initiates the same lattice transformation as observed in the previous case (see figure 6). The process leads again to a local reversal of stacking of the (111) planes and disintegration of the original GB. The boundary plane in the vicinity of the interaction site decomposes into two short segments which are inclined by 90 and 45 degrees to the original boundary plane [see figure7(e)]. The horizontal segment, which coincides with the dislocation glide plane, is a $\Sigma3(\bar{1}\bar{1}2)$. The other segment is a general boundary which joins the dislocation core with the original GB. The Burgers vector of the dislocation is distributed along both segments and the whole configuration can be considered as a transformed dislocation core. Due to the complex atomic structure of this arrangement it is however difficult to obtain more detailed information about this spreading. Upon further increase of the applied stress the configuration gradually traverses across the GB and starts to extend further into the neighboring grain [figure 7(c)]. The origins of this behavior can be again traced to the low barrier for the shuffling of atoms along the [111] direction and the underestimation of the $\Sigma3(11\bar{2})$ GB energy.

In case D, the orientation of the grains for the applied shear stress is in the TW/ATW sense. The dislocation therefore arrives at the boundary with its low stress side first [26, 54]. In this case no lattice transformation takes place and the dislocation is transmitted through the GB leaving it basically intact. The transmission is however not a continuous process. Upon reaching the GB the edge dislocation is first blocked and does not move further [figure 8(f)]. With additional increase of the applied stress the dislocation gradually penetrates the GB but remains attached to it [figure 8(g)]. Only after reaching a critical stress level the dislocation detaches from the GB and glides away [figure 8(h)].

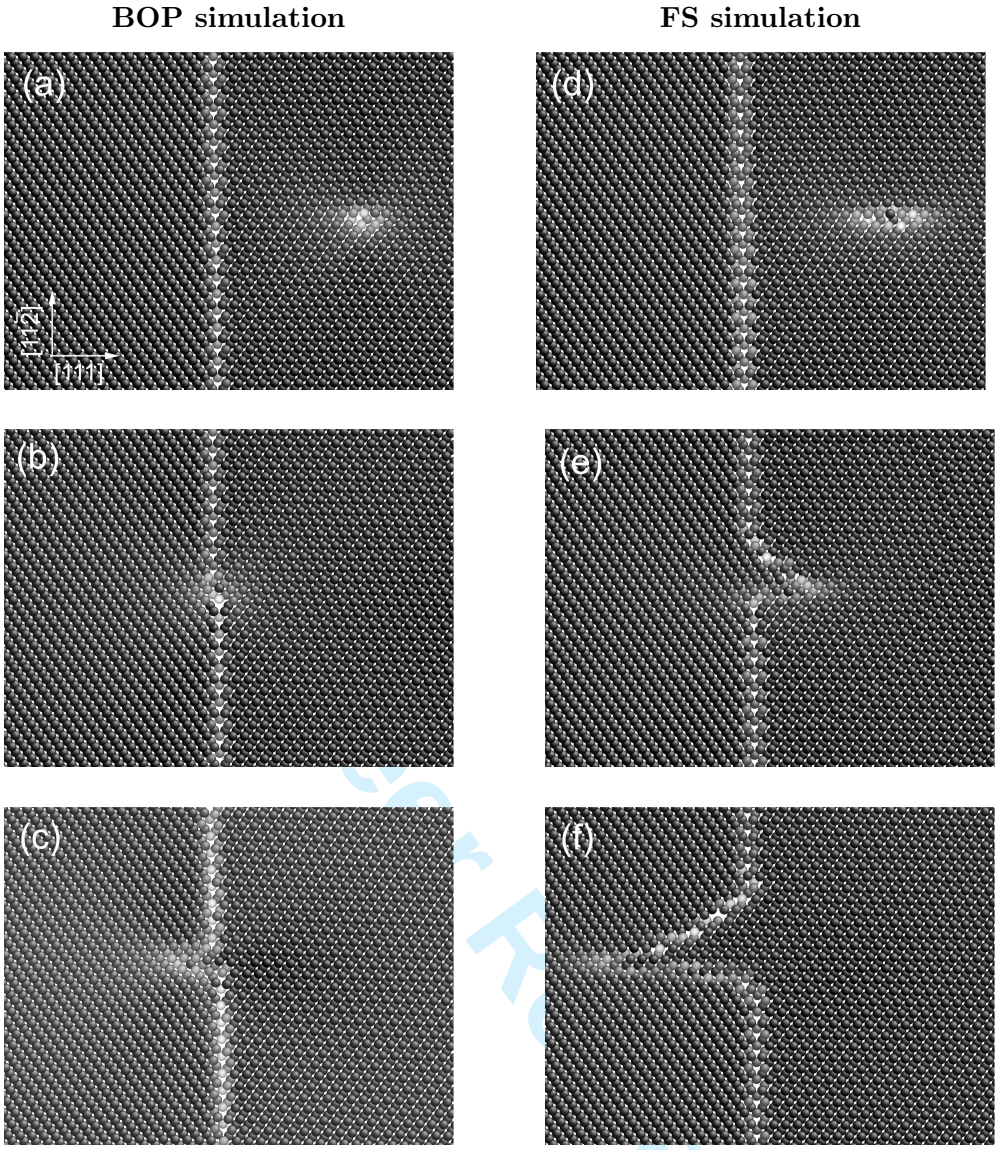

Figure 7. DGB interaction between the 1/2[111] edge dislocation gliding on a (11$\bar{2}$) plane in the ATW direction and the Σ3(111) GB.

4. Discussion and conclusions

The atomistic simulations performed in this work raise two main questions. The first concerns the reliability of the calculations as the obtained results depend sensitively on the employed interatomic potential. The second pertains to the present understanding of the DGB interactions – the investigated twin GBs present effective barriers to the motion of slip dislocations even though according to geometrical and stress criteria they should be transparent for the dislocations in the configurations studied here.

The problem of reliability and transferability lies in the heart of all theoretical descriptions of interatomic interactions. While it is expected that a model will provide reliable results if it is applied in environments not too dissimilar from those used for its fitting, with increasing complexity of the investigated problem the reliability becomes uncertain. The borderline between reliable and uncertain simulation outcome is however often difficult to locate. In the case of bcc transition metals the central-force character of the FS potential does not correspond to the physical reality of the chemical bonding. Nevertheless, the potential has been successfully

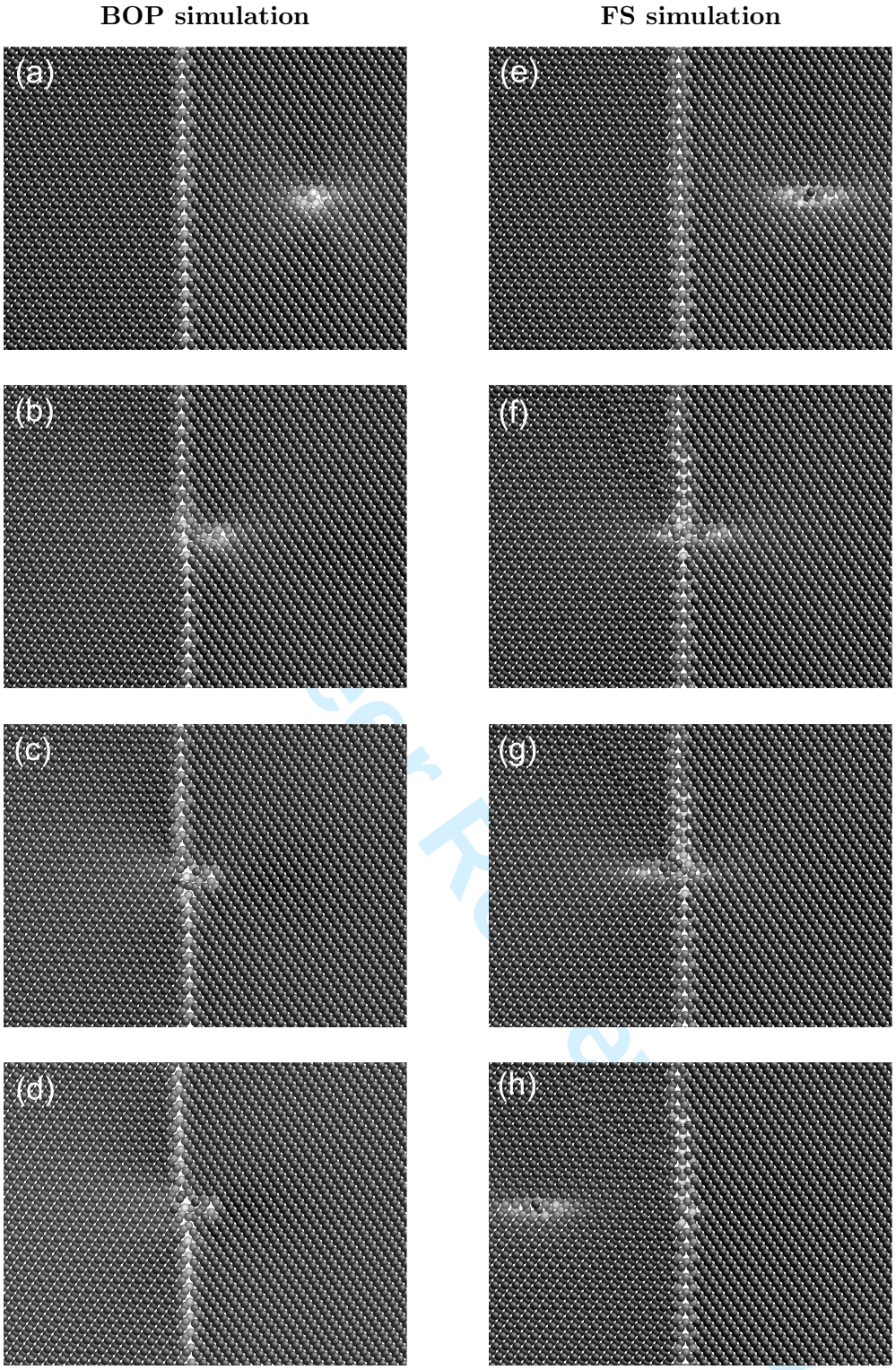

Figure 8. DGB interaction between the 1/2[111] edge dislocation gliding on a $(11\bar{2})$ plane in the TW direction and the $\Sigma 3(111)$ GB.

applied in a number of studies [26, 32, 56, 57] and its reliability deteriorates only in complex situations such as DGB interactions. It is important to emphasize that also for the BOP scheme there is no *a priori* guarantee that it is fully transferable to other configurations since the model is also fitted to a finite set of *ab initio* and/or experimental data. However, since it is based on quantum mechanical principles we anticipate that the BOP scheme is robust and reliable. This was confirmed not

only in the present but also in a number of previous studies [36, 38, 39]

From our analyses it is obvious that the origins of the different behavior of the two models can be traced back to relatively simple features, which can be validated using first-principles methods. This is an optimistic message for future developments. With the knowledge of their limitations the simple empirical potentials remain to be a useful tool. Due to their simplicity and computational efficiency they can be applied in sampling or test studies. Recent advances in development of new hybrid schemes provide additional promising ways to overcome the inherent limitations of simple empirical potentials by merging them with more sophisticated methods [58].

As was found in several recent studies [21, 23, 26], DGB interactions appear to be more complicated than previously thought. Even in the ideal cases studied here, where the dislocation line lies parallel to the GB plane and the glide plane continues through the boundary, the interactions are strongly influenced by processes occurring at the atomic level. In contrary to the existing empirical criteria, all our BOP simulations predict the GBs to be impenetrable obstacles for moving dislocations. In the case of the $1/2[111]$ screw dislocation and the $\Sigma3(11\bar{2})$ GB the dislocation immediately dissociates upon entering the GB. While the screw dislocation cannot split into partial dislocation in the bulk crystal, the dissociation is possible at the GB since the partial dislocations are admissible defects at the boundary. The dissociation is driven by a significant reduction of the elastic energy. Subsequent glide of the twinning dislocations along the boundary plane is associated with a formation of a step in the GB plane with magnitude of two $\{112\}$ interplanar spacings. In the remaining DGB cases involving edge dislocations local atomic interactions within the boundary are responsible for strong pinning of the dislocations making them sessile.

FS simulations show that a large variety of scenarios is possible in the DGB interactions. In case A the absorbed screw dislocation dissociates in agreement with the BOP simulation. It may be surprising that both FS and BOP results are consistent even though the core structure of the screw dislocation and the GB energy are not reproduced correctly by FS. The agreement is in this case therefore likely to be attributed to the energy balance rather than to atomistic effects. In the remaining cases the dislocation is at first blocked by the GB but with increasing applied stress it penetrates the boundary and continues its glide. The transmission process in cases B and C triggers a nucleation of other events which cause the original GB to disintegrate and effectively lead to a GB migration. Finally, in case D the dislocation is transmitted through the GB leaving it essentially intact in agreement with the empirical criteria. Even though the outcome of the DGB interactions in the last three cases is influenced by artefacts of the FS potential the information that different outcomes are possible is valuable. It is possible that the interatomic interactions in other materials resemble more those described by the employed FS potential leading to similar interaction mechanisms as those observed here.

In summary, our atomistic simulations show that the empirical criteria for dislocation transmission, which consider mainly the geometrical relationship between slip planes in neighboring grains, are not generally valid and the atomic level mechanisms play an important role in DGB interactions. The outcome of the reaction depends sensitively on the atomic rearrangements in the vicinity of the absorption site, which are determined by the properties of the atomic interactions through the interatomic potential. A correct description of interatomic interaction is therefore crucial for a reliable prediction of DGB interactions.

Acknowledgments

We greatly acknowledge financial support from the German Science Foundation (DFG), projects GU 367/25 and MR 22/5-1.

References

[1] J. P. Hirth and J. Lothe. *Theory of Dislocations*. Wiley-Interscience, New York, 1982.
[2] A. P. Sutton and R. W. Balluffi. *Interfaces in Crystalline Materials*. Oxford University Press, Oxford, 1995.
[3] Z. Shen, R.H. Wagoner, and W.A.T. Clark. *Scripta Metall.*, 20:921, 1986.
[4] T.C. Lee, I.M. Robertson, and H.K. Birnbaum. *Scripta Metall.*, 23:799, 1989.
[5] J.C. Huang and G.T. Gray. *Mater. Sci. Eng. A*, 103:241, 1988.
[6] J.W. Christian and S. Mahajan. *Prog. Mater. Sci.*, 39(1-2):1, 1995.
[7] M. Polcarova, J. Gemperlova, J. Bradler, A. Jacques, A. George, and L. Priester. *Philos. Mag. A*, 78:105, 1998.
[8] B. W. Lagow, I. M. Robertson, M. Jouiad, D. H. Lassila, T. C. Lee, and H. K. Birnbaum. *Mater. Sci. Eng. A*, 309-310:445, 2001.
[9] J. Gemperlova, A. Jacques, A. Gemperle, and N. Zarubova. *Interf. Sci.*, 10:51, 2002.
[10] A. Gemperle, J. Gemperlova, and N. Zarubova. *Mater. Sci. Eng. A*, 387-389:46, 2004.
[11] A. Gemperle, N. Zarubova, and J. Gemperlova. *J. Mater. Sci.*, 40:3247, 2005.
[12] B.J. Pestman, J.T.M. De Hosson, V. Vitek, and F.W. Schapink. *Scripta Metall.*, 23:1431, 1989.
[13] B. J. Pestman, J. Th. M. DeHosson, V. Vitek, and F. W. Schapink. *Philos. Mag. A*, 64:951, 1991.
[14] A. Serra and D.J. Bacon. *Acta Metall. Mater.*, 43:4465, 1995.
[15] A. Serra and D.J. Bacon. *Philos. Mag. A*, 73:333, 1996.
[16] Y. W. Zhang and T. C. Wang. *Model. Simul. Mater. Sci. Eng.*, 4:231, 1996.
[17] M. de Koning, R.J. Kurtz, V.V. Bulatov, C.H. Henager, R.G. Hoagland, W. Cai, and M. Nomura. *J. Nucl. Mater.*, 323:281, 2003.
[18] D. Saraev and S. Schmauder. *Phys. Stat. Sol. (b)*, 240:81, 2003.
[19] A. Hasnaoui, P.M. Derlet, and H. Van Swygenhoven. *Acta Mater.*, 52:2251, 2004.
[20] C.H. Henager, R.J. Kurtz, and R.G. Hoagland. *Philos. Mag.*, 84:2277, 2004.
[21] Z.H. Jin, P. Gumbsch, E. Ma, K. Albe, K. Lu, H. Hahn, and H. Gleiter. *Scripta Mater.*, 54:1163, 2006.
[22] H. Jang and D. Farkas. *Mater. Lett.*, 61:868, 2007.
[23] T. Zhu, J. Li, A. Samanta, H.G. Kim, and S. Suresh. *Proc. Nat. Acad. Sci.*, 104:3031, 2007.
[24] M.P. Dewald and W.A. Curtin. *Modell. Simul. Mater. Sci. Eng.*, 15:S193, 2007.
[25] Z.H. Jin, P. Gumbsch, K. Albe, E. Ma, K. Lu, H. Gleiter, and H. Hahn. *Acta Mater.*, 56:1126, 2008.
[26] Y. Cheng, M. Mrovec, and P. Gumbsch. *Philos. Mag.*, 88:547, 2008.
[27] P. M. Derlet, P. Gumbsch, R. Hoagland, J. Li, D. L. McDowell, H. Van Swygenhoven, and J. Wang. *MRS Bull.*, 34:184, 2009.
[28] R.W. Margevicius, J. Riedle, and P. Gumbsch. *Mat. Sci. Eng. A*, 270:197–209, 1999.
[29] A. Serra and D.J. Bacon. *Z. Metallk.*, 95:4, 2004.
[30] A. Serra and D.J. Bacon. *Mater. Sci. Eng. A*, 400-401:496, 2005.
[31] R. G. Hoagland, R. J. Kurtz, and C. H. Henager. *Scripta Mater.*, 50:775, 2004.
[32] Y. Cheng, M. Mrovec, and P. Gumbsch. *MAter. Sci. Eng. A*, 483-484:329, 2008.
[33] I. H. Katzarov, M. J. Cawkwell, A. T. Paxton, and M. W. Finnis. *Philos. Mag.*, 87(12):1795, 2007.
[34] M. W. Finnis and J. E. Sinclair. *Philos. Mag. A*, 50:45, 1984.
[35] G. J. Ackland and R. Thetford. *Philos. Mag. A*, 56:15, 1987.
[36] M. Mrovec, R. Gröger, A.G. Bailey, D. Nguyen-Manh, C. Elsässer, and V. Vitek. . *Phys. Rev. B*, 75:104119, 2007.
[37] A. G. Marinopoulos, V. Vitek, and A. E. Carlsson. *Philos. Mag. A*, 72:1311, 1995.
[38] T. Ochs, C. Elsässer, M. Mrovec, V. Vitek, J. Belak, and J. A. Moriarty. *Philos. Mag. A*, 80:2405, 2000.
[39] M. Mrovec, D. Nguyen-Manh, D. G. Pettifor, and V. Vitek. *Phys. Rev. B*, 69:094115, 2004.
[40] V. Vitek. *Philos. Mag.*, 84:415, 2004.
[41] V. Vitek and V. Paidar. *Dislocations in Solids*, volume 14, page 441. Oxford, 2008.
[42] D. G. Pettifor. *Phys. Rev. Lett.*, 63:2480, 1989.
[43] M. Aoki, P. Gumbsch, and D. G. Pettifor. In T. Terakura and H. Akai, editors, *Interatomic Potentials and Structural Stability*, volume 114, page 23. Springer, Berlin, 1993.
[44] A. P. Horsfield, A. M. Bratkovsky, D. G. Pettifor, and M. Aoki. *Phys. Rev. B*, 53(3):1656–1666, 1996.
[45] J. F. Peck and D. A. Thomas. *Trans. TMS-AIME*, 221:1240, 1961.
[46] P. F. Browning, C. L. Briant, K. Rajan, and B. A. Knudsen. *Eng. Failure Anal.*, 2:105, 1995.
[47] M. Mrovec, T. Ochs, C. Elsässer, V. Vitek, D. Nguyen-Manh, and D. Pettifor. *Z. Metallkd.*, 94:244, 2003.
[48] V. Vitek, R. C. Perrin, and D. K. Bowen. *Philos. Mag. A*, 21:1049, 1970.
[49] P. D. Bristowe and A. G. Crocker. *Philos. Mag.*, 31:503, 1975.
[50] M. Yamaguchi and V. Vitek. *Philos. Mag.*, 34:1, 1976.
[51] S. Ogata, J. Li, and S. Yip. *Phys. Rev. B*, 71:224102, 2005.
[52] J. W. Christian. In *Proc. 3rd Int. Conf. on Reinstoffe in Wissenschaft und Technik*, page 263, Berlin, 1970. Akademie-Verlag.
[53] Ju Li. *Modell. Simul. Mater. Sci. Eng.*, 11(2):173, 2003.
[54] M. Yamaguchi and V. Vitek. *J. Phys. F: Metal Phys.*, 5:1, 1975.

[55] M. Yamaguchi and V. Vitek. *J. Phys. F: Metal Phys.*, 5:11, 1975.
[56] S. Kohlhoff, P. Gumbsch, and H. F. Fischmeister. *Philos. Mag. A*, 64(4):851–878, 1991.
[57] K. Ito and V. Vitek. *Philos. Mag. A*, 81:1387, 2001.
[58] G. Csanyi, T. Albaret, M. C. Payne, and A. De Vita. *Phys. Rev. Lett.*, 93:175503, 2004.

Philosophical Magazine
Vol. 00, No. 00, 21 March 2009, 1–14

RESEARCH ARTICLE

Interactions between lattice dislocations and twin boundaries in tungsten: A comparative atomistic simulation study

M. Mrovec[a,b]* , C. Elsässer[a,b] and P. Gumbsch[a,b]

[a]IZBS, University of Karlsruhe, Kaiserstr. 12, 76131 Karlsruhe, Germany
[b]Fraunhofer Institute for Mechanics of Materials IWM, Wöhlerstr. 11, 79108 Freiburg, Germany

(*June 23, 2009*)

Plastic deformation of polycrystalline materials is largely controlled by the interaction between lattice dislocations and grain boundaries. The atomistic details of these interactions are however difficult to discern even by advanced high-resolution electron microscopy methods. In this paper we study several interactions of screw and edge dislocations with two symmetric tilt grain boundaries in the body-centred cubic metal tungsten by atomistic simulations. Two distinct models of interatomic interactions are applied - an empirical Finnis-Sinclair (FS) potential and a bond-order potential (BOP), which is based on quantum mechanical principles within the tight-binding electronic-structure theory. Our study shows that the outcome of the interactions is sensitive to the employed interatomic potential. Origins of the deviating behavior can be traced to differences in the description of atomic bonding by the two potentials. Independent of the employed interatomic potential, the simulations reveal that simple empirical criteria for dislocation transmission, which are based on geometry and stress arguments only, do not apply in general. Instead, in most cases processes occuring at the atomic level play a decisive role in determination of the underlying mechanisms of dislocations/grain-boundary interactions.

1. Introduction

When a polycrystalline metal undergoes plastic deformation, a large number of lattice dislocations impinge on grain boundaries (GBs) and interact with them. It has been observed experimentally that the interactions can result in impediment, transmission, absorption and reemission, or even reflection of dislocations [1, 2]. Unfortunately, little information is available about details of these processes at the atomic scale and only simple empirical criteria based on elementary geometry and stress factors have been proposed to predict the outcome of the dislocation/grain-boundary (DGB) interactions [3, 4]. While these criteria apply in some cases, a number of experimental [5–11] and theoretical [12–27] studies have shown that they are not valid in general and that the mechanisms of the DGB interactions are influenced by processes occuring at the atomic level.

In this work we investigate several DGB interactions in the bcc transition metal tungsten by atomistic simulations. Tungsten was chosen as our model material because of its peculiar mechanical behavior, which is controlled to a great extent by the structure and properties of extended defects, namely dislocation cores and grain boundaries. Depending on external conditions such as temperature, strain rate, or load orientation this transition metal can deform plastically by slip or deformation twinning or it can fracture by predominantly intergranular cleavage [28]. Properties

*Corresponding author. Email: matous.mrovec@iwm.fraunhofer.de

ISSN: 1478-6435 print/ISSN 1478-6443 online

DOI: 10.1080/1478643YYxxxxxxxx
http://www.informaworld.com

of dislocations, GBs, and details of mutual interactions between these extended defects are therefore of great interest since they may provide valuable information about conditions under which the competing deformation mechanisms take place.

The most important precursor of all atomistic simulations is a reliable description of interatomic interactions. Calculations of complex phenomena such as the DGB interactions require large simulation blocks and careful handling of boundary conditions. These stringent computational demands necessitate employment of empirical interatomic potentials instead of accurate first-principles electronic structure methods. To our knowledge almost all previous DGB simulations were performed with simple empirical potentials of the embedded-atom-method or Finnis-Sinclair (FS) type [12–17, 20–27, 29–32] with the exception of a recent work of Katzarov et al. on TiAl [33].

In the present paper we perform the simulations with two distinct models of interatomic interactions – an empirical Finnis-Sinclair potential [34, 35] and a recently developed bond-order potential (BOP) [36]. The FS potential is a many-body central-force scheme which has been used extensively in atomistic studies of extended defects in metals because of its simplicity and computational efficiency. Nevertheless, it is unable to describe properly the directional covalent bonds that are primarily responsible for structural and cohesive properties of bcc transition metals [36–41]. In order to validate FS results we therefore repeated the simulations with the BOP model, which is based on the real-space parameterized tight-binding (TB) method and provides implicitly a correct description of the angular character of bonding originating from d-electrons. An important advantage of the BOP scheme for simulations of extended defects and their interactions is that unlike classical TB models it scales linearly with the size of system since the diagonalization of the Hamiltonian matrix is replaced by direct calculation of the bond order in real space [42–44].

The main goals of the present work are twofold. First, we investigate the atomic-level mechanisms associated with the DGB interaction processes and compare the simulation results with predictions of the empirical criteria for dislocation transmission. Second, we examine if the outcome of the interactions depends on the interatomic potential employed and analyze underlying causes of eventual differences.

2. Simulation methodology

The DGB interactions were investigated for two symmetric tilt grain boundaries with a common $[\bar{1}10]$ tilt axis, namely, $\Sigma3(11\bar{2})$ and $\Sigma3(111)$. These GBs were chosen as model systems since extensive plastic deformation of bcc metals (e.g. during wire drawing) leads to a strong preferential $\langle 110 \rangle$ texture [45, 46]. Both GBs are high-angle GBs with a high density of coincidence sites and well defined equilibrium atomic structures. Their energies are however largely different (see below) and they can be therefore considered as representative cases of low and high energy GBs.

Configurations investigated in this work present rather special cases among possible DGB interactions in which the cross slip should encounter only a small resistance. In all our simulations the dislocation line lies parallel to the GB plane while the glide plane, i.e. the maximum resolved shear stress (MRSS) plane on which the dislocation is forced to glide, is always perpendicular to the GB plane. Because of the mirror-symmetrical structure of both GBs the glide plane continues through the GB into the other grain and the slip systems in both grains are therefore completely equivalent. Based on geometry considerations, the GBs in this case should

Table 1. Main characterictics of the four DGB configurations investigated in this work (see also figure 1).

Case	GB	Dislocation type	Slip systems in the grains
A	$\Sigma3(11\bar{2})$	screw	$[111](\bar{1}10)$ / $[11\bar{1}](\bar{1}10)$
B	$\Sigma3(111)$	edge	$[111](\bar{1}10)$ / $[11\bar{1}](\bar{1}10)$
C	$\Sigma3(111)$	edge	$[\bar{1}\bar{1}\bar{1}](\bar{1}\bar{1}2)_{\mathrm{ATW}}$ / $[\bar{1}\bar{1}1](112)_{\mathrm{TW}}$
D	$\Sigma3(111)$	edge	$[111](\bar{1}\bar{1}2)_{\mathrm{TW}}$ / $[11\bar{1}](112)_{\mathrm{ATW}}$

not act as obstacles to slip propagation because no residual GB dislocations are necessary to compensate for a change of the slip system.

For the chosen GBs there exist four such cases of DGB interactions, in which the $1/2\langle111\rangle$ dislocation of either pure screw or pure edge type impinges in parallel orientation on the GB. The four possibilities are described in table 1. In case A, a $1/2[111]$ screw dislocation gliding on a $(\bar{1}10)$ plane interacts with the $\Sigma3(11\bar{2})$ GB. In the remaining three cases an edge dislocation with the same Burgers vector gliding on either $(\bar{1}10)$ or $(\bar{1}\bar{1}2)$ planes interacts with the $\Sigma3(111)$ GB. For the $\{112\}$ glide planes it is necessary to distinguish between the twinning (TW) and antitwinning (ATW) directions. Since the $(\bar{1}\bar{1}2)$ plane is not a mirror plane the shearing of the crystal as well as the dislocation glide in opposite $1/2[111]$ directions are not equivalent. Furthermore, even though the $(\bar{1}\bar{1}2)$ plane continues through the GB the sense of shear is reversed, i.e. the TW sense in the left bicrystal changes to the ATW sense in the right bicrystal and vice versa. These two possibilities need to be treated separately and correspond to cases C and D.

The computational procedure was the same in all simulations. Initially, the GBs were created in the centre of the simulation cell and they were fully relaxed to their equilibrium configurations. After the static relaxation of the GB atomic structure either a perfect screw or edge dislocation with the $1/2\langle111\rangle$ Burgers vector was introduced in the middle of one of the grains. At this distance no attractive or repulsive forces were detected between the dislocation and the GB in any of the investigated systems.

With the dislocations present, the blocks were again fully relaxed. During the relaxation the positions of the dislocation cores remained at their initial elastic centers. It should be noted that tungsten is almost elastically isotropic and that incompatibily stresses at GBs are therefore negligible. Consequently, there are no long-range elastic forces on the dislocations near the GBs.

In the final step, a homogeneous shear strain was imposed on the simulation block, corresponding to a shear stress as prescribed by anisotropic elasticity theory. The shear stress was applied in the direction of the Burgers vector in such a way that the dislocation was forced to move towards the GB. The shear strain was gradually increased in small increments and the block was fully relaxed after each step so that the simulations were done effectively at 0 K.

The simulation setup with the sense of shear for both dislocation types is shown schematically in figure 1. The size of the simulation box was typically 15 nm $\times$ 10 nm in the x and y directions and the number of atoms ranged between 5 and 10 thousand. We carried out additional simulations with larger blocks using only the FS potential but did not find any size effect. Periodic boundary conditions were imposed along the z direction parallel to the dislocation line while fixed boundary conditions were used in the perpendicular x and y directions. The block in the x and y directions then consisted of an active region, in which all the atoms are fully relaxed, and an fixed region where the atoms are permanently displaced in accordance with the anisotropic elastic field of the dislocation. In order to allow the GB dislocations to move freely along the GB, simulations with free top and bottom surfaces were also tested. Again, the results were qualitatively the same as

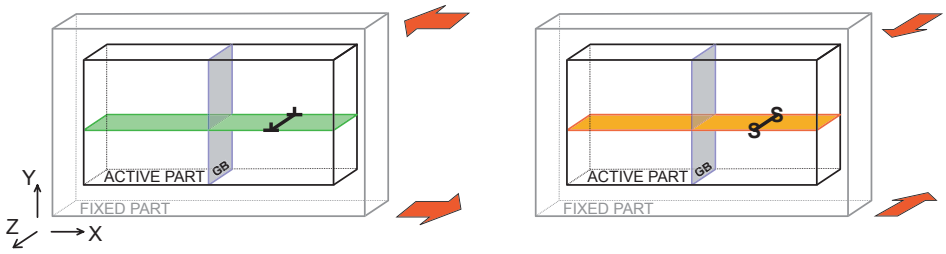

Figure 1. A schematic diagram of the simulation setup for the DGB interactions with edge and screw dislocations; the sense of applied shear is marked by arrows.

those with fixed boundaries.

3. Results

3.1. *Properties of the grain boundaries*

Since the atomic structure and energetics of the GBs may influence the outcome of the DGB interactions we computed first several characteristic properties of the two GBs using both FS and BOP schemes and compared them to results of benchmark first-principles density-functional theory (DFT) calculations [36, 47]. Here, we focus mainly on the $\Sigma3(11\bar{2})$ GB since, as will be discussed later, the differences in the description of this boundary by the two interatomic potentials are likely to be linked to differences in the observed DGB interactions.

The $\Sigma3(11\bar{2})$ GB is associated with deformation twins in bcc metals and is therefore frequently present in materials deformed at low temperatures or high strain rates [6]. Due to its regular atomic structure and bulk-like atomic density it is the lowest energy boundary among the [110] symmetric tilt GBs in bcc transition metals. The structure and energetics of this GB have been investigated extensively in the past for various bcc metals, both theoretically and experimentally (see, e.g., Refs. [37, 47–51] and references therein). A general result of all previous studies is that there exist two possible equilibrium configurations of this boundary, whose energies are nearly degenerate. The first configuration is a mirror symmetric structure corresponding to the coincidence site lattice interface [2]. The second configuration is obtained from the first one by displacing the upper grain with respect to the lower grain parallel to the boundary plane by the vector $\mathbf{t} = 1/12[111]$. The two structures are known as "reflection" and "isosceles" GBs [49], respectively, and are shown in figure 2.

The [111] lateral grain translation not only distinguishes the two low-energy GB structures but is of primary interest because it coincides with the direction of the twinning shear during deformation twinning. The computed energy profiles associated with the lateral translation of the two grains in the [111] direction over the whole GB period are plotted in figure 2. The curves in the figure represent the variation of the energy for rigid relative displacements of the grains without any atomic relaxation. The full symbols mark the energies of three high-symmetry translation states with all atomic positions relaxed. Figure 2 shows that except of the two low-energy configurations there exists another symmetry-dictated metastable configuration of this boundary, which can be obtained from the isosceles structure by a translation $\mathbf{t} = 1/4[111]$. This transition structure corresponds to an energy maximum and is therefore a hypothetical configuration which is unlikely to be present in the real material. This configuration may be however encountered as a transition state during shearing of the crystal.

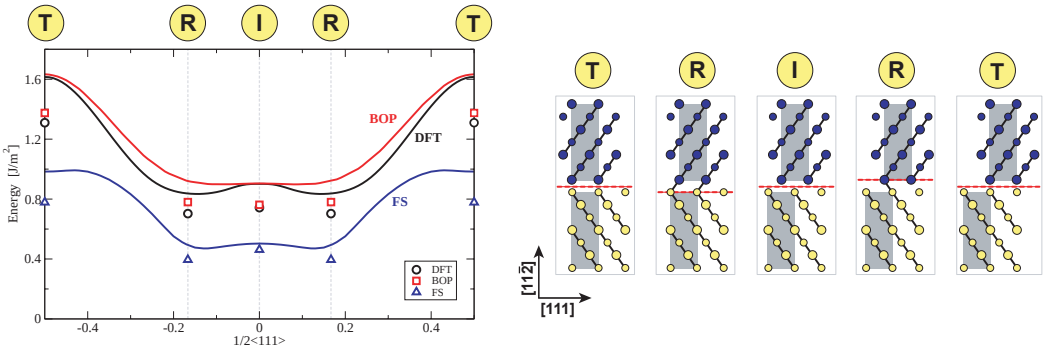

Figure 2. Energy of the $\Sigma3(11\bar{2})$ GB as a function of lateral displacement the grains along the [111] direction. The curves correspond to rigid relative displacements of the grains without any relaxation and the full symbols to fully relaxed symmetry structures. The corresponding atomic structures of the metastable GBs along the tilt axis are depicted next to the graph. Atoms with different radii lie in different $(\bar{1}10)$ planes; symbols R, I, and T denote reflection, isosceles, and transition structures, respectively.

Table 2. Comparison of GB energies for the $\Sigma3(11\bar{2})$ and $\Sigma3(111)$ boundaries calculated by different methods. For the $\Sigma3(11\bar{2})$ GB energies of the reflection (R), isosceles (I), transition (T) structures, and the difference between T and R structures are listed separately. All values are in mJ/m^2

GB	DFT	BOP	FS
$\Sigma3(11\bar{2})$			
(R)eflection	703	780	395
(I)soscelles	743	762	462
(T)ransition	1310	1375	778
Δ_{T-R}	607	595	383
$\Sigma3(111)$			
3D PBCs (12 atom cell)	2274	2195	1401
3D PBCs (24 atom cell)	2350	2409	2337
2D PBCs	–	2398	2364

Since the calculations can be carried out also with accurate first-principles methods, they serve as a valuable benchmark case for validation of the employed interatomic potentials (cf. Refs [38, 47]). The comparison in figure 2 shows that for rigid displacements the BOP results follow closely those of DFT both qualitatively and quantitatively. The FS potential mimics correctly the shape of the energy profile but the absolute values are underestimated by almost factor of two. After relaxation the DFT calculations yield the reflection structure to be the most stable. According to the BOP calculations, both the isosceles and reflection structures are metastable with the isosceles structure favored by 18 mJ/m^2 over the reflection structure (see table 2). Hence, in the prediction of the ground state structure DFT and BOP give contradictory results, although the energy difference is very small and represents only about 2 % of the GB energy. The FS potential gives correctly the order of the three GB structures but significantly underestimates their absolute energies. Additionally, the energy barrier related to the shear strength of the GB along the [111] direction, i.e., the energy difference between the transition and reflection structures, is also predicted to be about 40% lower than in DFT and BOP calculations (see table 1). The reason for these strong underestimations is the central-force character of the FS potential. In the $\Sigma3(11\bar{2})$ boundary the separation of the first and second neighbours is the same as in the ideal crystal and thus only the third and more distant neighbours contribute to the GB energy.

In contrast to the $\Sigma3(11\bar{2})$ GB, the atomic structure of the $\Sigma3(111)$ deviates markedly from the bulk bcc environment and its energy is therefore significantly higher than that of the former boundary (see table 2). We found that all three

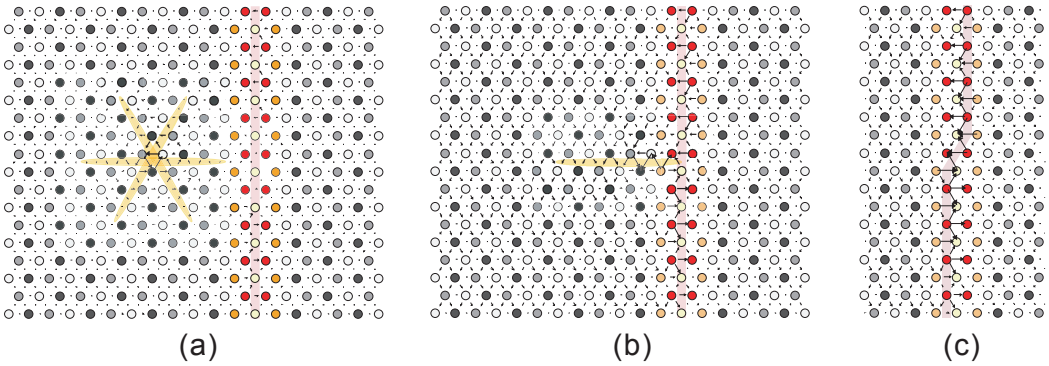

Figure 3. Initial (a), intermediate (b), and final (c) simulation snapshots from the DGB interaction between the 1/2[111] screw dislocation gliding on the $(\bar{1}10)$ plane and the $\Sigma3(11\bar{2})$ GB (BOP simulations). The pictures are $\langle 111\rangle$ views with the $(\bar{1}10)$ glide plane lying horizontally. The arrows were obtained using the standard method of differential displacements [48] and correspond to atomic displacements in the $\langle 111\rangle$ direction. The nonplanar structure of the dislocation core and position of the GB plane are highlited.

computational methods agree very well in predicting the GB energy as well as the atomic structure provided that the boundary is well isolated (does not interact with itself). In DFT calculations, periodic supercells containing two identical GBs are necessary and the cells must be large enough to avoid mutual interactions between the boundaries. For the $\Sigma3(111)$ GB a supercells with 12 atoms does not satisfy this requirement since the GBs are separated by only three $\{111\}$ planes and start to interact. This interaction leads to a reduction of the GB energy. The decrease is only marginal in DFT and BOP calculations, but in the case of FS potential it leads to unphysical changes in the structure of the bulk region between the GBs and a significant drop in the energy. This behavior is again likely to be caused by insufficient transferability of the FS potential to considerably distorted environments. Table 2 shows that for the 24 atom supercell, in which the distance beween periodic images of the GBs is sufficiently large, the agreement between all three methods is excellent. For BOP and FS potentials these results are also consistent with calculations done using 2D periodic boundary conditions (PBCs) parallel to the interface in which the GB is effectively embedded in two infinite bulk halfcrystals.

3.2. *Case A: Interaction between screw dislocation gliding on* $\{\bar{1}10\}$ *plane and* $\Sigma3(11\bar{2})$ *GB*

The first DGB interaction is the only one among the four investigated cases where a screw dislocation appears. It has been known for long time that properties of screw dislocations in bcc materials differ markedly from those of edge dislocations [52]. Characteristic features of the screw dislocations, such as low mobility, high intrinsic lattice friction (Peierls stress), and thermally activated motion via formation of kinks, have their origin in a three-dimensional non-planar structure of the dislocation core (for review see e.g. Refs. [40, 41, 52] and article by Vitek in this special issue).

Since the two employed interatomic potentials predict qualitatively different core structures of the 1/2[111] screw dislocation [36, 40] it may be expected that this difference will be also reflected in the DGB interaction process. Our calculations however reveal that the interaction between the 1/2[111] screw dislocation gliding on the $(\bar{1}10)$ plane and the $\Sigma3(11\bar{2})$ GB proceeds identically for both potentials. Figure 3 depicts initial, intermediate, and final configurations of the simulations using the standard method of differential displacements [48]. The screw dislocation starts moving towards the boundary [figure 3(a)] at the same critical stress as in

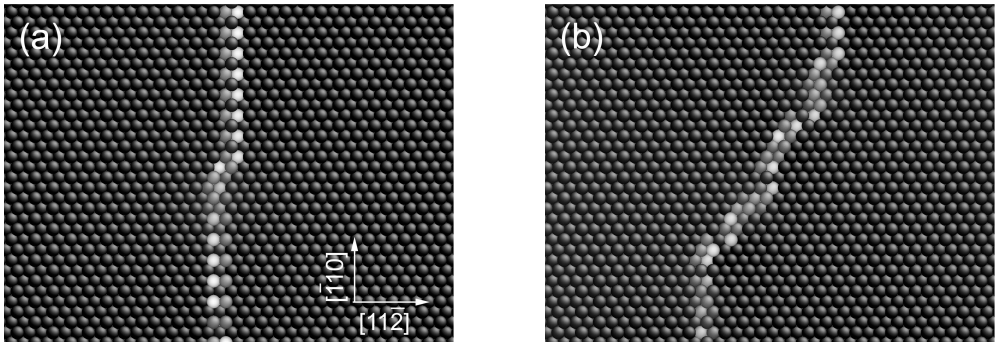

Figure 4. Structure of the $\Sigma3(11\bar{2})$ GB after interaction with one (a) and eight (b) 1/2[111] screw dislocations (FS simulation).

the bulk crystal, which confirms that the GB does not influence the Peierls barrier of the dislocation. When the dislocation reaches the GB [figure 3(b)] it is absorbed and immediately dissociates into three partial dislocations, each with the Burgers vector of 1/6[111]. These dislocations, also known as twinning dislocations which propagate deformation twins [1, 6], are geometrically admissible defects at this interface and can move conservatively along the GB plane. After the dissociation, a mutual repulsion forces two of the twinning dislocations to glide in opposite directions on neighboring $(11\bar{2})$ GB planes. As a result of this process the GB above and below the absorption site migrates in opposite directions and an embryo of a new GB, which contains the remaining twinning dislocation, forms at the interaction site [figure 3(c)].

While BOP calculations are computationally demanding, the efficiency of the FS potential enables us to study a more realistic case of DGB interaction with multiple incoming dislocations. Using free top and bottom surfaces of the simulation block so that the GB dislocations can leave the block we gradually inserted eight dislocations in the vicinity of the boundary. The simulations show that also the subsequent interactions proceed in a similiar way as with a single dislocation, i.e., by absorption and dissociation of the incoming lattice dislocations. Figures 4(a) and 4(b) depict the snapshots of the simulation block after absorption of one and eight dislocations, respectively, using the local von Mises shear strain invariant [53]. Remains of the original straight boundary plane can be seen only in the top and bottom regions of figure 4(b) with a newly formed GB in between. The new GB is inclined by about 60 degress to the original GB and is therefore itself an imperfect $\Sigma3\{112\}$ twin GB.

3.3. *Case B: Interaction between edge dislocation gliding on* $\{\bar{1}10\}$ *plane and* $\Sigma3(111)$ *GB*

Unlike the 1/2[111] screw dislocations, the edge dislocations have planar cores and, consequently, their mobility is several orders of magnitude higher than the mobility of the screws [1]. Both BOP and FS potentials give a planar core structure for the 1/2[111] edge dislocation spread on the $(\bar{1}10)$ plane and differ only in the extension of the core.

Surprisingly, despite the similar dislocation cores structures the BOP and FS potentials give qualitatively different results for the interaction between the 1/2[111] edge dislocation gliding on the $(\bar{1}10)$ plane and the $\Sigma3(111)$ GB. The initial and final snapshots of the simulation box from both simulations are shown in figure 5. In the BOP simulation the dislocation is again blocked by the GB and stays embedded in the boundary even when the shear stress is increased up to 6% of the shear elastic modulus C_{44}. The same GB in the FS simulations presents a much weaker obstacle for the dislocation. Initially, the dislocation is also absorbed at

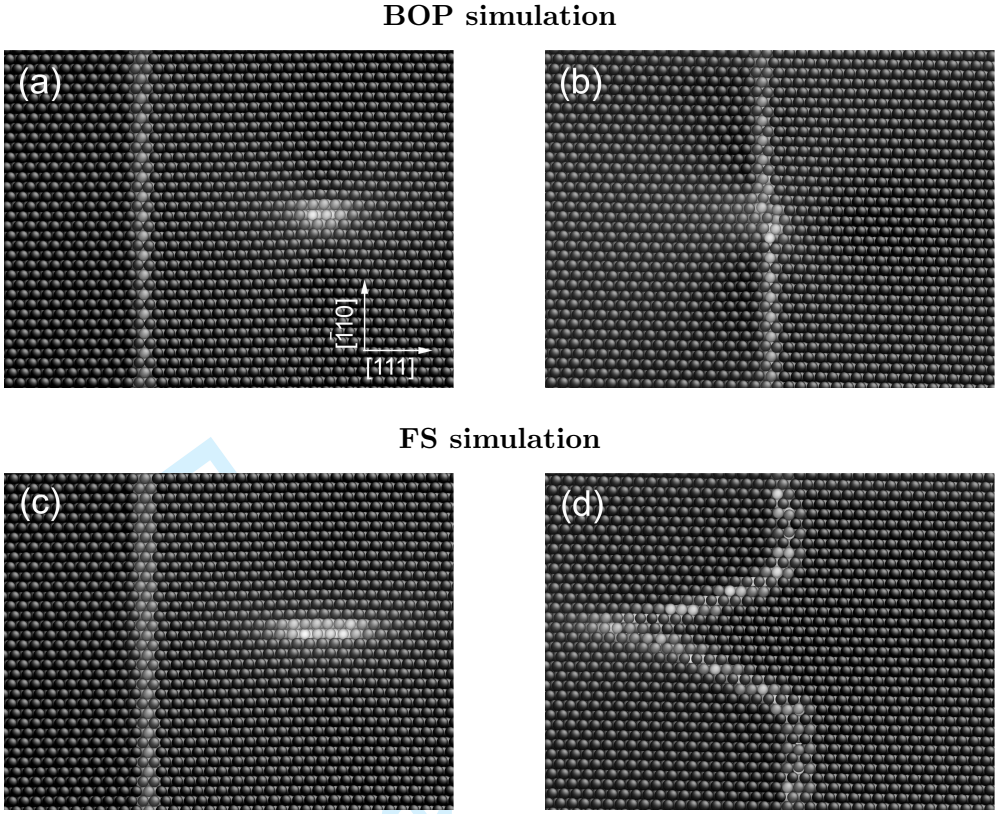

Figure 5. Initial, (a) and (c), and final, (b) and (d), simulation snapshots from the DGB interaction between the 1/2[111] edge dislocation gliding on the ($\bar{1}$10) plane and the Σ3(111) GB calculated using BOP and FS potentials, respectively.

the GB but at the applied stress of about 3% of C_{44} it detaches from the GB and starts to glide into the neighboring grain. As shown in figure 5(d), the outgoing edge dislocation triggers a wave of local changes in the crystal, which follow the moving dislocation and effectively destroy the original GB. The disintegration of the GB is caused by ongoing transformations of the ABCBAC stacking of the (111) planes across the GB to the ideal ABCABC stacking of the bulk bcc lattice. The transformation can be achieved by translating atoms on neighboring ($\bar{1}$10) planes in opposite directions by the vector ±1/6[111]. This atomic shuffling, which is schematically shown in figure 6, is associated with an energy barrier. Calculated profiles of this barrier in the ideal bcc structure are shown also in figure 6. We can see that while the magnitude of the barrier is around 4 eV according to DFT and BOP calculations, with the FS potential it reaches only 1.5 eV. The presence of the absorbed dislocation and the effect of the applied stress probably decrease the barrier even further and lead thus to initiation of the transformation.

3.4. *Cases C and D: Interaction between edge dislocation gliding on* {211} *plane and* Σ3(111) *GB*

It was shown already more than thirty years ago by Yamaguchi and Vitek [54, 55] that the core of the 1/2⟨111⟩ edge dislocation lying on a {112} plane is also planar. Since the core is predominantly confined to a single plane it can be described as a continuous distribution of the Burgers vector [26]. This distribution is asymmetric due to the well known twinning-antitwinning asymmetry of shear on {112} planes and may be interpreted as a dissociation into two fractional dislocations with the Burgers vectors 1/6⟨111⟩ and 1/3⟨111⟩ [52]. The dislocation therefore behaves differently when gliding in opposite ⟨111⟩ directions and the two cases need to be

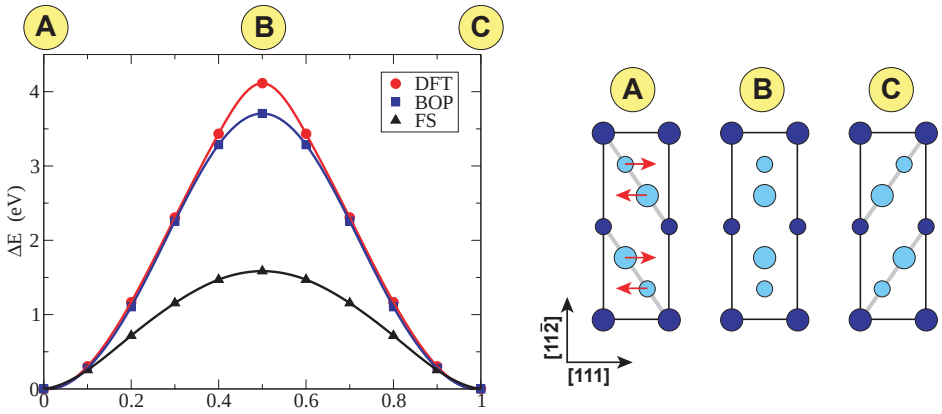

Figure 6. Calculated energy barriers associated with shuffling of atoms along the [111] direction on neighboring {$\bar{1}$10} planes. The atomic configuration corresponding to the initial, transition, and final states are shown schematically on the right.

treated separately.

Similarly as in case B, BOP and FS simulations give qualitatively different results even though the dislocation core structures from the two potentials are very similar. In BOP simulations, the result of the DGB interaction is independent of the sense of shearing. The dislocation is always trapped at the GB and does not propagate to the neighboring grain. A sequence of simulation snapshots from cases C and D are shown in figures 7 and 8, respectively.

In contrast, the outcome of the interaction in FS simulations depends on the crystal orientation. In case C, which corresponds to the ATW/TW orientation of the grains, the dislocation starts moving in the right grain in the antitwinning direction while the sense of shear in the neighboring grain is reversed to the twinning direction. Figure 7(e) shows that when the dislocation approaches the GB the compressive stress field above its glide plane initiates the same lattice transformation as observed in the previous case (see figure 6). The process leads again to a local reversal of stacking of the (111) planes and disintegration of the original GB. The boundary plane in the vicinity of the interaction site decomposes into two short segments which are inclined by 90 and 45 degrees to the original boundary plane [see figure7(e)]. The horizontal segment, which coincides with the dislocation glide plane, is a $\Sigma3(\bar{1}\bar{1}2)$. The other segment is a general boundary which joins the dislocation core with the original GB. The Burgers vector of the dislocation is distributed along both segments and the whole configuration can be considered as a transformed dislocation core. Due to the complex atomic structure of this arrangement it is however difficult to obtain more detailed information about this spreading. Upon further increase of the applied stress the configuration gradually traverses across the GB and starts to extend further into the neighboring grain [figure 7(c)]. The origins of this behavior can be again traced to the low barrier for the shuffling of atoms along the [111] direction and the underestimation of the $\Sigma3(11\bar{2})$ GB energy.

In case D, the orientation of the grains for the applied shear stress is in the TW/ATW sense. The dislocation therefore arrives at the boundary with its low stress side first [26, 54]. In this case no lattice transformation takes place and the dislocation is transmitted through the GB leaving it basically intact. The transmission is however not a continuous process. Upon reaching the GB the edge dislocation is first blocked and does not move further [figure 8(f)]. With additional increase of the applied stress the dislocation gradually penetrates the GB but remains attached to it [figure 8(g)]. Only after reaching a critical stress level the dislocation detaches from the GB and glides away [figure 8(h)].

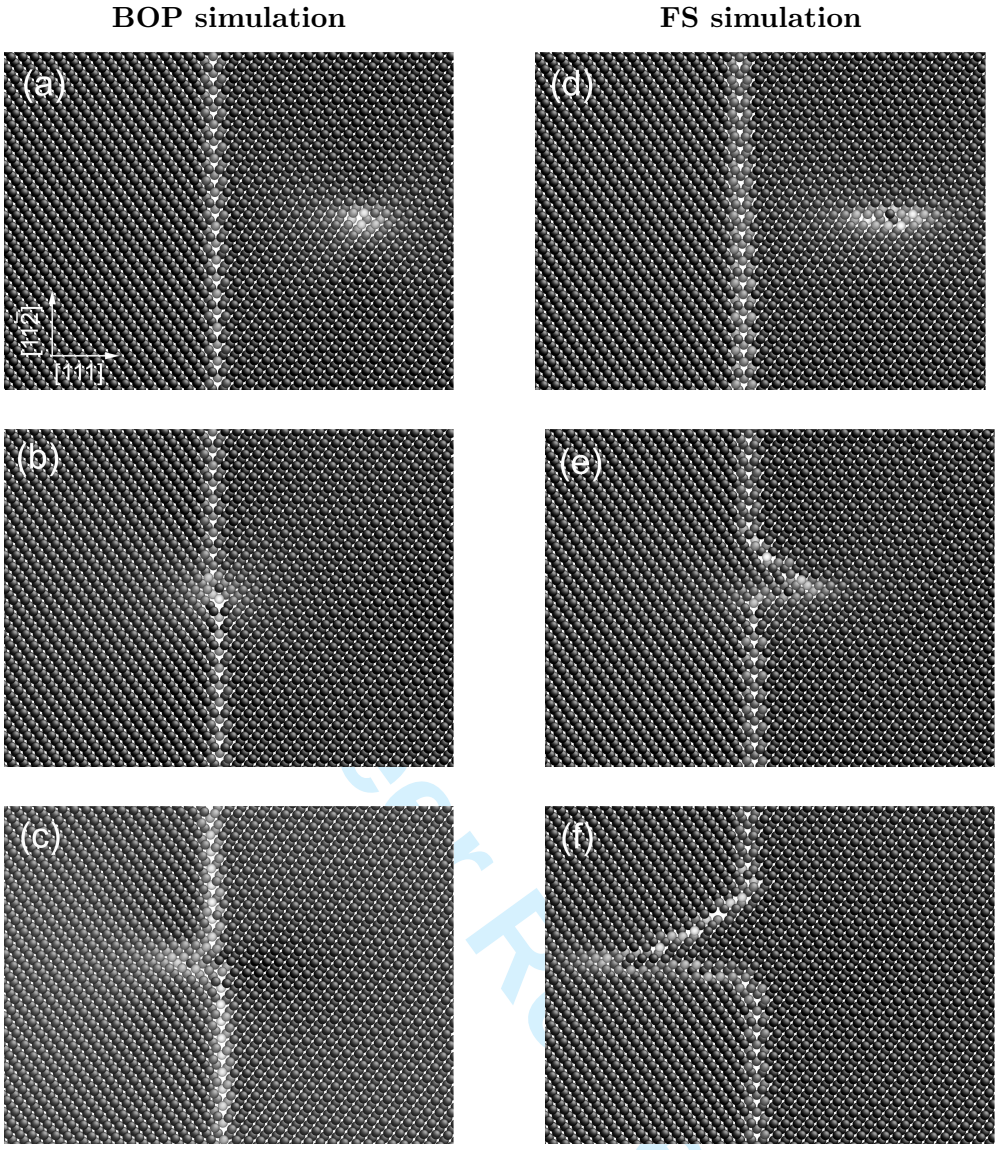

Figure 7. DGB interaction between the 1/2[111] edge dislocation gliding on a (11$\bar{2}$) plane in the ATW direction and the Σ3(111) GB.

4. Discussion and conclusions

The atomistic simulations performed in this work raise two main questions. The first concerns the reliability of the calculations as the obtained results depend sensitively on the employed interatomic potential. The second pertains to the present understanding of the DGB interactions – the investigated twin GBs present effective barriers to the motion of slip dislocations even though according to geometrical and stress criteria they should be transparent for the dislocations in the configurations studied here.

The problem of reliability and transferability lies in the heart of all theoretical descriptions of interatomic interactions. While it is expected that a model will provide reliable results if it is applied in environments not too dissimilar from those used for its fitting, with increasing complexity of the investigated problem the reliability becomes uncertain. The borderline between reliable and uncertain simulation outcome is however often difficult to locate. In the case of bcc transition metals the central-force character of the FS potential does not correspond to the physical reality of the chemical bonding. Nevertheless, the potential has been successfully

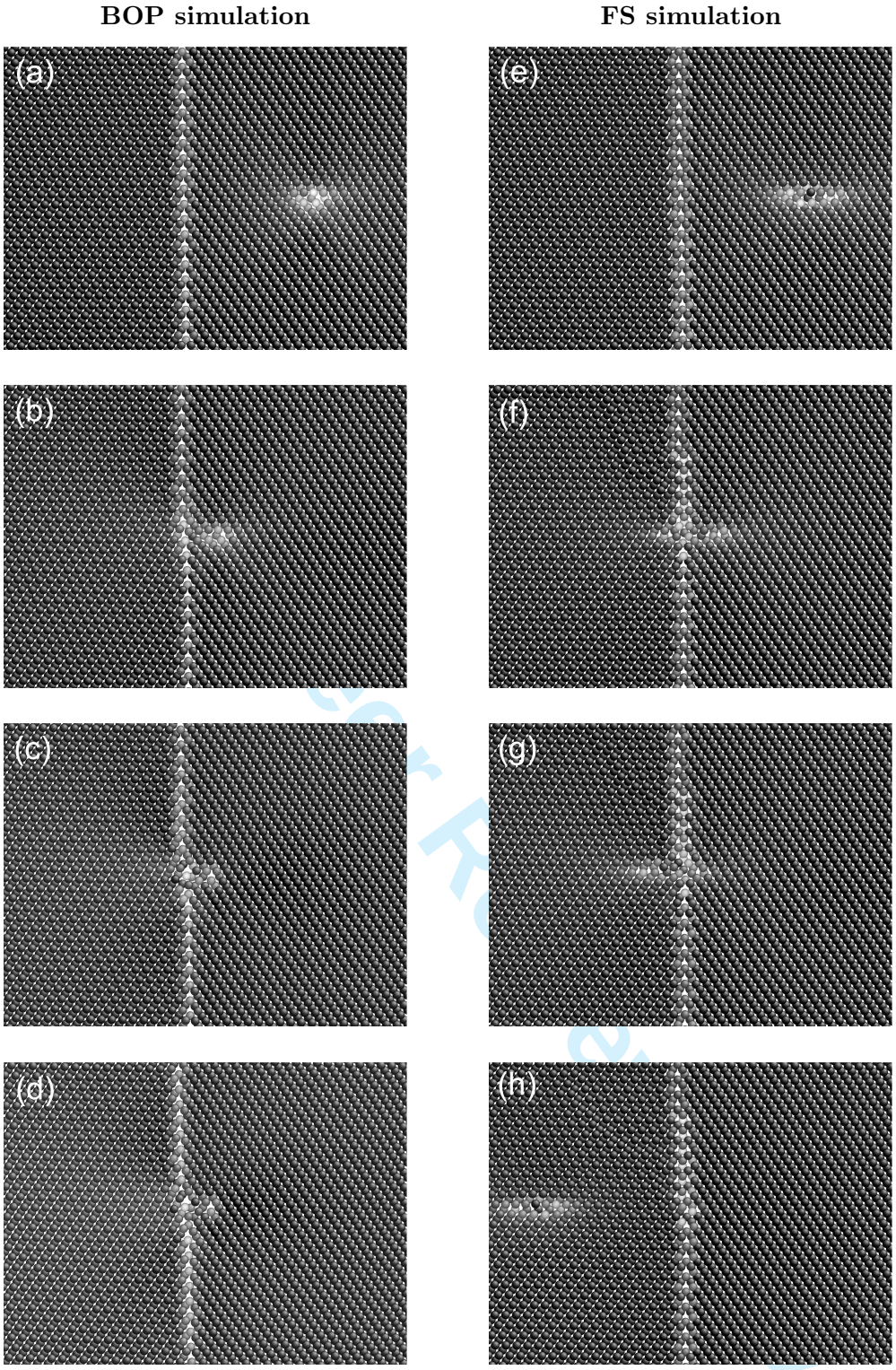

Figure 8. DGB interaction between the 1/2[111] edge dislocation gliding on a $(11\bar{2})$ plane in the TW direction and the Σ3(111) GB.

applied in a number of studies [26, 32, 56, 57] and its reliability deteriorates only in complex situations such as DGB interactions. It is important to emphasize that also for the BOP scheme there is no *a priori* guarantee that it is fully transferable to other configurations since the model is also fitted to a finite set of *ab initio* and/or experimental data. However, since it is based on quantum mechanical principles we anticipate that the BOP scheme is robust and reliable. This was confirmed not

only in the present but also in a number of previous studies [36, 38, 39]

From our analyses it is obvious that the origins of the different behavior of the two models can be traced back to relatively simple features, which can be validated using first-principles methods. This is an optimistic message for future developments. With the knowledge of their limitations the simple empirical potentials remain to be a useful tool. Due to their simplicity and computational efficiency they can be applied in sampling or test studies. Recent advances in development of new hybrid schemes provide additional promising ways to overcome the inherent limitations of simple empirical potentials by merging them with more sophisticated methods [58].

As was found in several recent studies [21, 23, 26], DGB interactions appear to be more complicated than previously thought. Even in the ideal cases studied here, where the dislocation line lies parallel to the GB plane and the glide plane continues through the boundary, the interactions are strongly influenced by processes occurring at the atomic level. In contrary to the existing empirical criteria, all our BOP simulations predict the GBs to be impenetrable obstacles for moving dislocations. In the case of the $1/2[111]$ screw dislocation and the $\Sigma3(11\bar{2})$ GB the dislocation immediately dissociates upon entering the GB. While the screw dislocation cannot split into partial dislocation in the bulk crystal, the dissociation is possible at the GB since the partial dislocations are admissible defects at the boundary. The dissociation is driven by a significant reduction of the elastic energy. Subsequent glide of the twinning dislocations along the boundary plane is associated with a formation of a step in the GB plane with magnitude of two $\{112\}$ interplanar spacings. In the remaining DGB cases involving edge dislocations local atomic interactions within the boundary are responsible for strong pinning of the dislocations making them sessile.

FS simulations show that a large variety of scenarios is possible in the DGB interactions. In case A the absorbed screw dislocation dissociates in agreement with the BOP simulation. It may be surprising that both FS and BOP results are consistent even though the core structure of the screw dislocation and the GB energy are not reproduced correctly by FS. The agreement is in this case therefore likely to be attributed to the energy balance rather than to atomistic effects. In the remaining cases the dislocation is at first blocked by the GB but with increasing applied stress it penetrates the boundary and continues its glide. The transmission process in cases B and C triggers a nucleation of other events which cause the original GB to disintegrate and effectively lead to a GB migration. Finally, in case D the dislocation is transmitted through the GB leaving it essentially intact in agreement with the empirical criteria. Even though the outcome of the DGB interactions in the last three cases is influenced by artefacts of the FS potential the information that different outcomes are possible is valuable. It is possible that the interatomic interactions in other materials resemble more those described by the employed FS potential leading to similar interaction mechanisms as those observed here.

In summary, our atomistic simulations show that the empirical criteria for dislocation transmission, which consider mainly the geometrical relationship between slip planes in neighboring grains, are not generally valid and the atomic level mechanisms play an important role in DGB interactions. The outcome of the reaction depends sensitively on the atomic rearrangements in the vicinity of the absorption site, which are determined by the properties of the atomic interactions through the interatomic potential. A correct description of interatomic interaction is therefore crucial for a reliable prediction of DGB interactions.

Acknowledgments

We greatly acknowledge financial support from the German Science Foundation (DFG), projects GU 367/25 and MR 22/5-1.

References

[1] J. P. Hirth and J. Lothe. *Theory of Dislocations*. Wiley-Interscience, New York, 1982.
[2] A. P. Sutton and R. W. Balluffi. *Interfaces in Crystalline Materials*. Oxford University Press, Oxford, 1995.
[3] Z. Shen, R.H. Wagoner, and W.A.T. Clark. *Scripta Metall.*, 20:921, 1986.
[4] T.C. Lee, I.M. Robertson, and H.K. Birnbaum. *Scripta Metall.*, 23:799, 1989.
[5] J.C. Huang and G.T. Gray. *Mater. Sci. Eng. A*, 103:241, 1988.
[6] J.W. Christian and S. Mahajan. *Prog. Mater. Sci.*, 39(1-2):1, 1995.
[7] M. Polcarova, J. Gemperlova, J. Bradler, A. Jacques, A. George, and L. Priester. *Philos. Mag. A*, 78:105, 1998.
[8] B. W. Lagow, I. M. Robertson, M. Jouiad, D. H. Lassila, T. C. Lee, and H. K. Birnbaum. *Mater. Sci. Eng. A*, 309-310:445, 2001.
[9] J. Gemperlova, A. Jacques, A. Gemperle, and N. Zarubova. *Interf. Sci.*, 10:51, 2002.
[10] A. Gemperle, J. Gemperlova, and N. Zarubova. *Mater. Sci. Eng. A*, 387-389:46, 2004.
[11] A. Gemperle, N. Zarubova, and J. Gemperlova. *J. Mater. Sci.*, 40:3247, 2005.
[12] B.J. Pestman, J.T.M. De Hosson, V. Vitek, and F.W. Schapink. *Scripta Metall.*, 23:1431, 1989.
[13] B. J. Pestman, J. Th. M. DeHosson, V. Vitek, and F. W. Schapink. *Philos. Mag. A*, 64:951, 1991.
[14] A. Serra and D.J. Bacon. *Acta Metall. Mater.*, 43:4465, 1995.
[15] A. Serra and D.J. Bacon. *Philos. Mag. A*, 73:333, 1996.
[16] Y. W. Zhang and T. C. Wang. *Model. Simul. Mater. Sci. Eng.*, 4:231, 1996.
[17] M. de Koning, R.J. Kurtz, V.V. Bulatov, C.H. Henager, R.G. Hoagland, W. Cai, and M. Nomura. *J. Nucl. Mater.*, 323:281, 2003.
[18] D. Saraev and S. Schmauder. *Phys. Stat. Sol. (b)*, 240:81, 2003.
[19] A. Hasnaoui, P.M. Derlet, and H. Van Swygenhoven. *Acta Mater.*, 52:2251, 2004.
[20] C.H. Henager, R.J. Kurtz, and R.G. Hoagland. *Philos. Mag.*, 84:2277, 2004.
[21] Z.H. Jin, P. Gumbsch, E. Ma, K. Albe, K. Lu, H. Hahn, and H. Gleiter. *Scripta Mater.*, 54:1163, 2006.
[22] H. Jang and D. Farkas. *Mater. Lett.*, 61:868, 2007.
[23] T. Zhu, J. Li, A. Samanta, H.G. Kim, and S. Suresh. *Proc. Nat. Acad. Sci.*, 104:3031, 2007.
[24] M.P. Dewald and W.A. Curtin. *Modell. Simul. Mater. Sci. Eng.*, 15:S193, 2007.
[25] Z.H. Jin, P. Gumbsch, K. Albe, E. Ma, K. Lu, H. Gleiter, and H. Hahn. *Acta Mater.*, 56:1126, 2008.
[26] Y. Cheng, M. Mrovec, and P. Gumbsch. *Philos. Mag.*, 88:547, 2008.
[27] P. M. Derlet, P. Gumbsch, R. Hoagland, J. Li, D. L. McDowell, H. Van Swygenhoven, and J. Wang. *MRS Bull.*, 34:184, 2009.
[28] R.W. Margevicius, J. Riedle, and P. Gumbsch. *Mat. Sci. Eng. A*, 270:197–209, 1999.
[29] A. Serra and D.J. Bacon. *Z. Metallk.*, 95:4, 2004.
[30] A. Serra and D.J. Bacon. *Mater. Sci. Eng. A*, 400-401:496, 2005.
[31] R. G. Hoagland, R. J. Kurtz, and C. H. Henager. *Scripta Mater.*, 50:775, 2004.
[32] Y. Cheng, M. Mrovec, and P. Gumbsch. *MAter. Sci. Eng. A*, 483-484:329, 2008.
[33] I. H. Katzarov, M. J. Cawkwell, A. T. Paxton, and M. W. Finnis. *Philos. Mag.*, 87(12):1795, 2007.
[34] M. W. Finnis and J. E. Sinclair. *Philos. Mag. A*, 50:45, 1984.
[35] G. J. Ackland and R. Thetford. *Philos. Mag. A*, 56:15, 1987.
[36] M. Mrovec, R. Gröger, A.G. Bailey, D. Nguyen-Manh, C. Elsässer, and V. Vitek. . *Phys. Rev. B*, 75:104119, 2007.
[37] A. G. Marinopoulos, V. Vitek, and A. E. Carlsson. *Philos. Mag. A*, 72:1311, 1995.
[38] T. Ochs, C. Elsässer, M. Mrovec, V. Vitek, J. Belak, and J. A. Moriarty. *Philos. Mag. A*, 80:2405, 2000.
[39] M. Mrovec, D. Nguyen-Manh, D. G. Pettifor, and V. Vitek. *Phys. Rev. B*, 69:094115, 2004.
[40] V. Vitek. *Philos. Mag.*, 84:415, 2004.
[41] V. Vitek and V. Paidar. *Dislocations in Solids*, volume 14, page 441. Oxford, 2008.
[42] D. G. Pettifor. *Phys. Rev. Lett.*, 63:2480, 1989.
[43] M. Aoki, P. Gumbsch, and D. G. Pettifor. In T. Terakura and H. Akai, editors, *Interatomic Potentials and Structural Stability*, volume 114, page 23. Springer, Berlin, 1993.
[44] A. P. Horsfield, A. M. Bratkovsky, D. G. Pettifor, and M. Aoki. *Phys. Rev. B*, 53(3):1656–1666, 1996.
[45] J. F. Peck and D. A. Thomas. *Trans. TMS-AIME*, 221:1240, 1961.
[46] P. F. Browning, C. L. Briant, K. Rajan, and B. A. Knudsen. *Eng. Failure Anal.*, 2:105, 1995.
[47] M. Mrovec, T. Ochs, C. Elsässer, V. Vitek, D. Nguyen-Manh, and D. Pettifor. *Z. Metallkd.*, 94:244, 2003.
[48] V. Vitek, R. C. Perrin, and D. K. Bowen. *Philos. Mag. A*, 21:1049, 1970.
[49] P. D. Bristowe and A. G. Crocker. *Philos. Mag.*, 31:503, 1975.
[50] M. Yamaguchi and V. Vitek. *Philos. Mag.*, 34:1, 1976.
[51] S. Ogata, J. Li, and S. Yip. *Phys. Rev. B*, 71:224102, 2005.
[52] J. W. Christian. In *Proc. 3rd Int. Conf. on Reinstoffe in Wissenschaft und Technik*, page 263, Berlin, 1970. Akademie-Verlag.
[53] Ju Li. *Modell. Simul. Mater. Sci. Eng.*, 11(2):173, 2003.
[54] M. Yamaguchi and V. Vitek. *J. Phys. F: Metal Phys.*, 5:1, 1975.

[55] M. Yamaguchi and V. Vitek. *J. Phys. F: Metal Phys.*, 5:11, 1975.
[56] S. Kohlhoff, P. Gumbsch, and H. F. Fischmeister. *Philos. Mag. A*, 64(4):851–878, 1991.
[57] K. Ito and V. Vitek. *Philos. Mag. A*, 81:1387, 2001.
[58] G. Csanyi, T. Albaret, M. C. Payne, and A. De Vita. *Phys. Rev. Lett.*, 93:175503, 2004.